University of Maribor
Faculty of Energy Technology

Journal of ENERGY TECHNOLOGY

Volume 14 / Issue 2
OCTOBER 2021
www.fe.um.si/en/jet.html

Journal of ENERGY TECHNOLOGY

VOLUME 14 / Issue 2

Revija Journal of Energy Technology (JET) je indeksirana v bazah INSPEC© in Proquest's Technology Research Database.

The Journal of Energy Technology (JET) is indexed and abstracted in database INSPEC© and Proquest's Technology Research Database.

JOURNAL OF ENERGY TECHNOLOGY

Tehnični urednik / TECHNICAL EDITOR

Sonja Novak

Tehnična podpora / TECHNICAL SUPPORT

Tamara BREČKO BOGOVČIČ

Izhajanje revije / PUBLISHING

Revija izhaja štirikrat letno v nakladi 100 izvodov. Članki so dostopni na spletni strani revije - www.fe.um.si/si/jet.html / The journal is published four times a year. Articles are available at the journal's home page - www.fe.um.si/en/jet.html.

Cena posameznega izvoda revije (brez DDV) / Price per issue (VAT not included in price): 50,00 EUR

Informacije o naročninah / Subscription information: http://www.fe.um.si/en/jet/subscriptions.html

Lektoriranje / LANGUAGE EDITING

TAIA INT d.o.o.

Oblikovanje in tisk / DESIGN AND PRINT

Foto Colarič, Boštjan Colarič s.p.

Naslovna fotografija / COVER PHOTOGRAPH

Jurij AVSEC

Oblikovanje znaka revije / JOURNAL AND LOGO DESIGN

Andrej PREDIN

Ustanovni urednik / FOUNDING EDITOR

Andrej PREDIN

Izdajanje revije JET finančno podpira Javna agencija za raziskovalno dejavnost Republike Slovenije iz sredstev državnega proračuna iz naslova razpisa za sofinanciranje domačih znanstvenih periodičnih publikacij / The Journal of Energy Technology is co-financed by the Slovenian Research Agency.

Spoštovani bralci revije Journal of energy technology (JET)

Nenadzorovana izraba fosilnih virov, večanje populacije človeštva, krčenje naravnih habitatov, velika industrializacija in s tem povezani izpusti toplogrednih plinov povzročajo svetu velike ekološke težave. Okoljske težave postajajo svetu največji izziv človeštva v bližnji prihodnosti. V mesecu novembru se bodo v Glasgowu na Škotskem zbrali svetovni voditelji na veliki podnebni konferenci COP 26. Na omenjeni konferenci bodo voditelji skušali skleniti nove zaveze, da bi dosegli cilj – zvišanje povprečne temperature svetu za največ 1,5 °C. Za dosego tega cilja bo v bližnji prihodnosti treba izvesti veliko ukrepov. V ta namen bodo morale države najti poti za precej večjo izrabo obnovljivih virov v povezavi s trajnostno naravnano družbo ob sočasni uporabi alternativnih energetskih tehnologij. Tudi učinkovita izraba energetskih virov na vseh področjih energetike lahko pripomore k boljšim rezultatom. Velika odgovornost za dosego teh ciljev pripada najrazvitejšim državam, ki so tudi največje porabnice energetskih virov. Srčno upam, da bo konferenca v Glasgowu uspešna in da se bodo svetovni voditelji zavedali svoje velike odgovornosti.

Jurij AVSEC
odgovorni urednik revije JET

Dear Readers of the Journal of Energy Technology (JET)

Unbridled use of fossil resources, increasing human population, depletion of natural habitats, large-scale industrialisation and related greenhouse gas emissions are causing major ecological problems throughout the world. Environmental problems will become the greatest global challenge for humanity in the near future. In November, world leaders will gather in Glasgow, Scotland for the major COP 26 climate conference, at which the leaders will try to make new commitments to achieve the goal of limiting the rise in the global average temperature to a maximum of 1.5 degrees Celsius. Many measures will need to be taken in the near future to achieve this goal. To this end, countries will need to find ways to make much greater use of renewables in conjunction with a sustainable society, while using alternative energy technologies. Efficient use of energy resources in all areas of energy can also contribute to even better results. Of course, the greatest responsibility for achieving these goals belongs to the most developed countries, which are also the largest consumers of energy resources. I sincerely hope that the Glasgow conference will be a success and that world leaders will be aware of their great responsibilities.

Jurij AVSEC
Editor-in-chief of JET

Table of Contents / Kazalo

Journal of Energy Technology

JET Volume 14 (2021) p.p. 11-19
Issue 2, October 2021
Type of article 1.01
www.fe.um.si/en/jet.html

3D COUPLED ELECTROMAGNETIC-THERMAL ANALYSIS OF A HYBRID ELECTROMAGNETIC SYSTEM WITH MAGNETIC FLUX MODULATION

3D ELEKTROMAGNETNA IN TOPLOTNA ANALIZA HIBRIDNEGA ELEKTROMAGNETNEGA SISTEMA Z MODULACIJO MAGNETNEGA PRETOKA

Ivan Hadzhiev[✉], Iosko Balabozov[1], Vultchan Gueorgiev[2], Ivan Yatchev[1]

Keywords: Coupled problems, finite element analysis, hybrid electromagnetic system, magnetic flux modulation, permanent magnets.

Abstract

This paper presents a study of the electromagnetic and thermal field of a new construction of a hybrid electromagnetic system with magnetic flux modulation. The numerical studies were realised using the finite element method. The coupled problem electromagnetic field-electric circuit-thermal field was solved. A computer model of the hybrid electromagnetic system was developed for the purpose of the study using the software programme COMSOL. Results for the distribution of the electromagnetic and thermal field in the hybrid electromagnetic system with magnetic modulation were obtained at different supply voltages.

[✉] Assoc. Prof. Ivan Hadzhiev, Technical University of Sofia, Plovdiv Branch, Department of Electrical Engineering, Tsanko Dyustabanov 25, 4000 Plovdiv, Bulgaria, Tel: +359 32 659 686, E-mail address: hadzhiev_tu@abv.bg

[1] Technical University of Sofia, Department of Electrical Apparatus, Technical University of Sofia, 8, Kliment Ohridski Blvd, 1000 Sofia, Bulgaria

[2] Technical University of Sofia, Department of Power Supply, Electrical Equipment and Electrical Transport, Technical University of Sofia, Kliment Ohridski 8, 1000 Sofia, Bulgaria

Povzetek

Prispevek predstavlja raziskavo elektromagnetnega in toplotnega polja nove konstrukcije hibridnega elektromagnetnega sistema z modulacijo magnetnega pretoka. Numerične raziskave so bile izvedene z metodo končnih elementov. Rešen je bil problem povezanega elektromagnega in toplotnega polja. Za namene raziskave je bil razviti računalniški model hibridnega elektromagnetnega sistema s programsko opremo COMSOL. Rezultati porazdelitve elektromagnetnega in toplotnega polja v hibridnem elektromagnetnem sistemu z magnetno modulacijo so bili pridobljeni pri različnih napajalnih napetostih.

1 INTRODUCTION

One of the main requirements when creating new devices is energy efficiency. In order to improve energy efficiency, new design solutions are being developed using new materials and technologies. In this regard, hybrid electromagnetic systems with magnetic flux modulation (HEMSMM) find wide application. HEMSMM have undergone a number of studies and patenting [1]-[6].

This paper describes the computer modelling of a new construction of HEMSMM developed and described in [7], [8], which was carried out by solving the coupled problem of electromagnetic field-electric circuit-thermal field in transient mode.

2 CONSTRUCTION OF THE STUDIED HEMSMM

The structure of the studied HEMSMM is shown in Fig. 1. It consists of a magnetic core, one input (control) coil, three output (signal) coils, two permanent magnets and an air gap. The magnetic core is made of ferrite with a cross-section of 20x10mm. The length of the air gap is 1mm. All the coils are made of a cylindrical copper conductor of diameter 0.56mm. The input coil 1 and the output coil 2 each have 200 turns. The other two output coils – 3 and 4 – each have 400 turns. The cross-section of the permanent magnets is 20x10mm, and their thickness is 2mm.

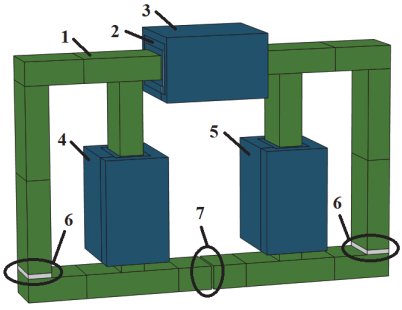

Figure 1: *Geometry of the studied construction of HEMSMM: 1 - ferromagnetic frame; 2 - input (control) coil 1; 3 - output (signal) coil 2; 4 - output (signal) coil 3; 5 - output (signal) coil 4; 6 - permanent magnets; 7 - air gap.*

3 MATHEMATICAL MODEL

To solve the coupled problem electromagnetic field-electric circuit-thermal field, the finite element method was used. The problem was solved in three steps. The equation of the electromagnetic field in steady state, created for permanent magnets, was solved in the first step. The permanent magnets were modelled with relative permeability μ_r = 1.05 and coercive force of 970 kA/m. The electric circuit was not involved in this step and the equation has the form:

$$\nabla \times (\mu^{-1} \nabla \times \boldsymbol{A} - \boldsymbol{M}) = 0, \tag{3.1}$$

where: $\boldsymbol{A}$ is the magnetic vector potential; $\boldsymbol{M}$ is the magnetisation; μ is the magnetic permeability.

The electromagnetic problem was solved by imposing the Dirichlet boundary condition on the boundary of the buffer zone.

The results of the static magnetic field were used as a starting condition for the second step. The coupled problem electromagnetic field-electric circuit in transient mode was solved in the second step. The equation for the electromagnetic field in transient mode is:

$$\sigma \frac{\partial \boldsymbol{A}}{\partial t} + \nabla \times (\mu^{-1} \nabla \times \boldsymbol{A} - \boldsymbol{M}) = N \frac{i(t)}{S}, \tag{3.2}$$

where: σ is the electrical conductivity of the material; N is number of turns of the coil; i is the current through the coil; S is the coil cross-section.

The inductance and the active resistance of the coils were obtained from the electromagnetic field interface and are directly employed in the electric circuit. Active loads are connected to the output coils. The equations of the four coils are:

$$u_1(t) = R_1 i_1(t) + \frac{\partial \psi_1}{\partial t}; \tag{3.3}$$

$$-\frac{\partial \psi_2}{\partial t} = R_2 i_2(t); \tag{3.4}$$

$$-\frac{\partial \psi_3}{\partial t} = R_3 i_3(t); \tag{3.5}$$

$$-\frac{\partial \psi_4}{\partial t} = R_4 i_4(t), \tag{3.6}$$

where: $u_1(t)$ is the voltage of coil 1; R_1 to R_4 are the active resistances of the coils; $i_1(t)$ to $i_4(t)$ are the currents through the coils; Ψ is the flux linkage.

The electric circuit used in the simulations is shown in Fig. 2.

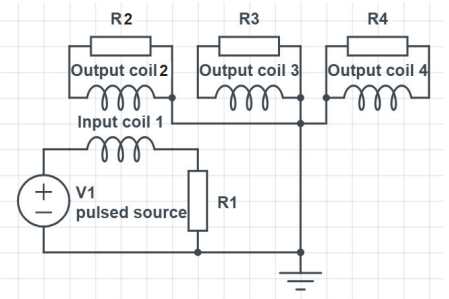

Figure 2: *Electric circuit used in the simulations*

The B-H curve of the magnetic core is shown in Fig. 3.

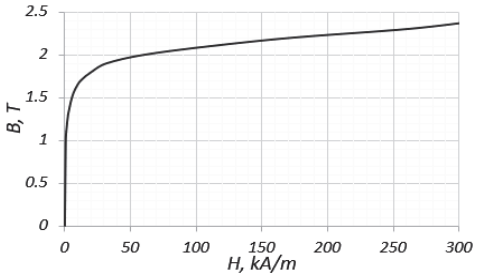

Figure 3: *B-H curve of the ferromagnetic material of the core*

From the solution to the electromagnetic problem, the volumetric loss density in the coils and the magnetic core are obtained. These losses are the sources of heat for the solution of the thermal problem, which is carried out in the third step. The thermal field is described by the equation of thermal conductivity in transient mode:

$$\rho c\left(\frac{\partial T}{\partial t}\right) = \nabla(\lambda \nabla T) + q, \tag{3.7}$$

where: T is the temperature; ρ is the density of the material; c is the specific heat; λ is the coefficient of thermal conductivity; q is the volumetric density of the heat sources.

The solution of the thermal problem is found under the following initial and boundary conditions:

- at time t=0 the ambient temperature is set to 20°C;

- heat transfer from the outer surfaces of the coils and the magnetic core to the environment through convection and radiation:

$$-\lambda\left(\frac{\partial T}{\partial n}\right) = h\left(T_s - T_{amb}\right); \tag{3.8}$$

$$\lambda\left(\frac{\partial T}{\partial n}\right) = \varepsilon k_B\left(T_s^4 - T_{amb}^4\right), \tag{3.9}$$

where: h is a coefficient of convection, defined by the criterion of Nuselt in the programme COMSOL; k_B=5.67x10^{-8} W/m^{2}K^{-4} is the constant of Stephan Boltzmann; ε is the emissivity; T_s is the temperature of the outer surface of the coils and the magnetic core; T_{amb} is the ambient temperature.

4 FINITE ELEMENT ANALYSIS

The numerical studies were conducted with the help of a 3D computer model in COMSOL [9]. The coupled problem electromagnetic field - electric circuit - thermal field in transient mode was solved. The finite element method was used to analyse the model and the resulting mesh is shown in Fig. 4.

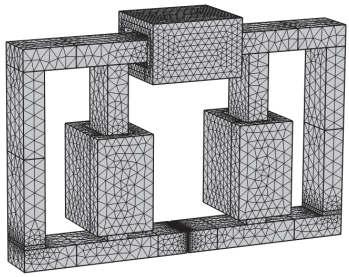

Figure 4: *Finite elements mesh*

5 NUMERICAL RESULTS

By using the developed 3D model of HEMSMM, the results for the electromagnetic and thermal fields were obtained at a frequency of 5kHz and different supply voltages of the input coil – 6V, 9V and 12V.

Fig. 5 and Fig. 6 illustrate the distribution of the magnetic field, while Fig. 7 and Fig. 8 show the input and output power at the 6V and 12V supply voltages respectively. Fig. 9 shows the thermal field distribution in HEMSMM at different supply voltages of the input coil and an operating time of 2h. Fig. 10 illustrates the transient mode of temperature rise in the coils and the magnetic core at different supply voltages of the input coil.

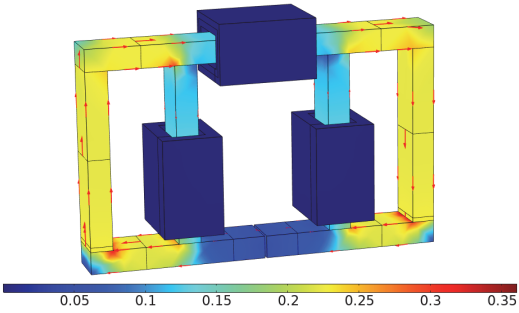

Figure 5: *Distribution of the magnetic flux density (T) in HEMSMM, when the input coils are not energised*

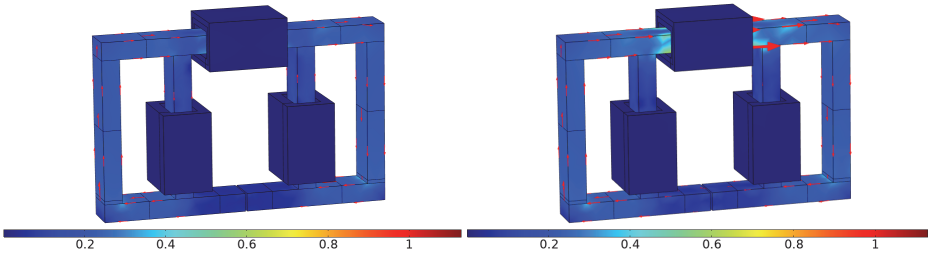

a) *b)*

Figure 6: *Distribution of the magnetic flux density (T) in HEMSMM, when the input coil is supplied with the following voltages: a) 6V; b) 12V*

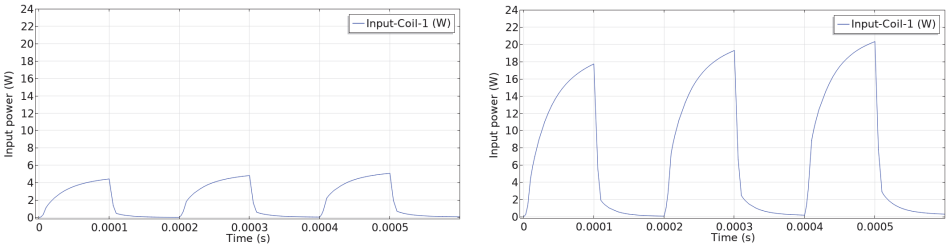

a) *b)*

Figure 7: *Input power at supply voltage of: a) 6V; b) 12V*

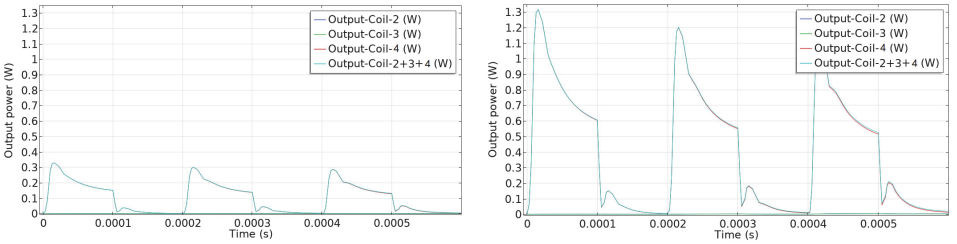

a) *b)*

Figure 8: *Output power at supply voltage of the input coil: a) 6V b) 12V*

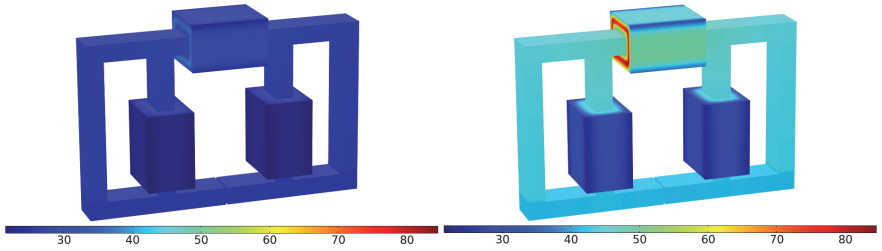

a) *b)*

Figure 9: *Thermal field distribution (°C) in HEMSMM at operating time 2h and supply voltages: a) 6V; b) 12V*

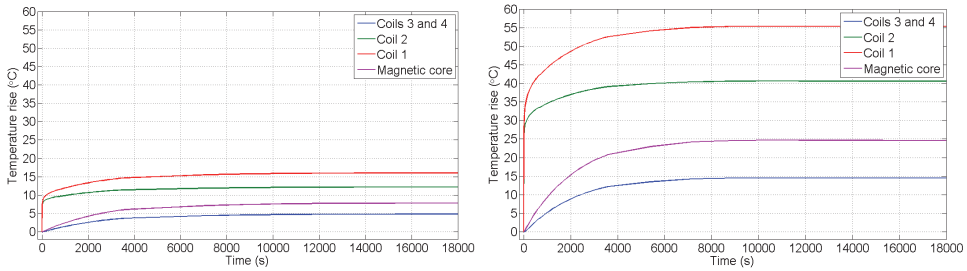

Figure 10: *Transient mode of temperature rise in the coils and the magnetic core of HEMSMM at supply voltages: a) 6V; b) 12V*

Fig. 11 illustrates the results obtained for the temperature rise in the coils and the magnetic core in transient mode at different supply voltages and a frequency of 5kHz.

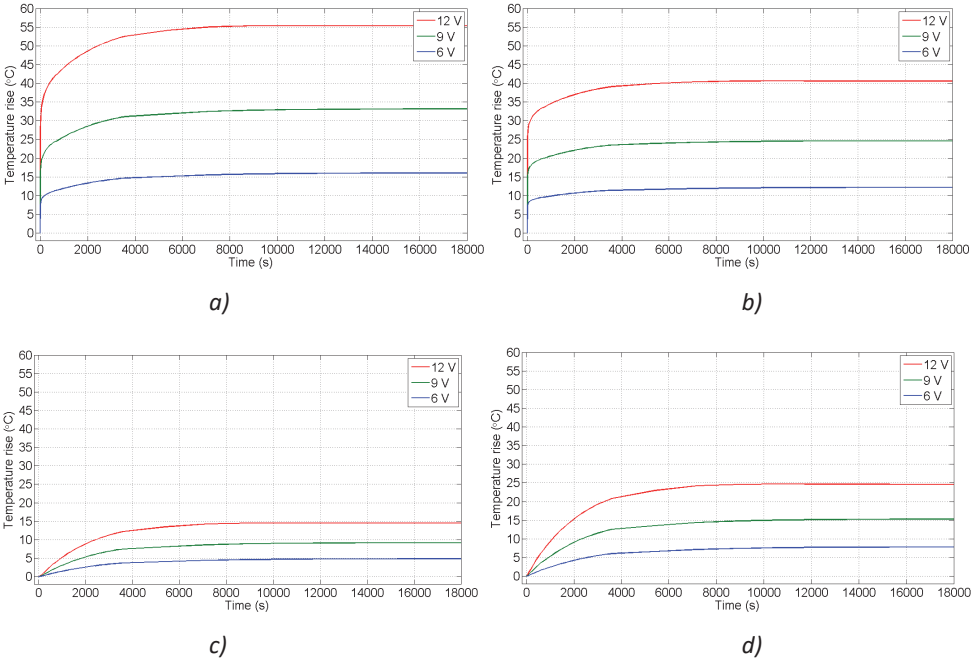

Figure 11: *Transient mode of temperature rise in: a) the input coil 1; b) the output coil 2; c) the output coils 3 and 4; d) the magnetic core*

6 CONCLUSION

Numerical studies of a new HEMSMM design were conducted at different supply voltages and results were obtained for the distribution of the magnetic and thermal fields.

As the value of the supply voltage increases, the input power, output power and the magnetic flux density in HEMSMM increase.

Due to the losses in the coils and the magnetic core, the HEMSMM temperature rise also increases with the increasing value of the supply voltage. When the supply voltage is doubled (from 6V to 12V), the temperature rise of the coils and the magnetic core increases about three-fold.

The greatest temperature rise occurs on the input coil 1, and the least on the two output coils 3 and 4. HEMSMM reaches a thermal steady-state after about 2 hours of operation.

The developed computer model can be used for optimisation of HEMSMM.

Acknowledgement

This research work is supported by the National Science Fund of the Bulgarian Ministry of Education and Science, Project No.DN 17/13.

References

[1] **S.V. Leonov, A.N. Zhiganov, B.M. Kerbel, D.F. Fedorov, Y.N. Makaseev, I.A. Kremlev:** *Analysis of the influence of permanent magnet geometry on the energy efficiency of electromechanical systems*, Russian Physics Journal, Vol.59, no.2, p.p.308-313, 2016

[2] **H. Kunel:** *Procedures and devices for energy production*, Patent DE3024814, 1982

[3] **J. Suarez:** *Estatico processor electrical power*, ES Patent 2265253 B1, 2008

[4] **R. Matsanov:** *Pulse generator*, Patent WO2010094993A1, 2010

[5] **A.S. Tatevosian, A.A. Tatevosian, V.N. Dorokhin:** *Permanent magnet machine*, RU Patent 2542322 C2, 2015

[6] **A. Gleich:** *Permanent magnet-driven current generator*, Patent application DE102014017612A1, 2016

[7] **I. Yatchev, I. Balabozov, K. Hinov, G. Georgiev, M. Minchev, I. Hadzhiev, V. Gueorgiev:** *Method and system for magnetic modulation*, Patent BG 67343 B1, 2021

[8] **I. Balabozov, D. Tomov, I. Yatchev, I. Hadzhiev, H. Brauer:** *Experimental study of the influence of some parameters on the characteristics of hybrid electromagnetic system with magnetic flux modulation*, 21st International Symposium on Electrical Apparatus and Technologies, SIELA 2020 – Proceedings, 2020

[9] *COMSOL Multiphysics 5.3 User's Guide*, COMSOL Inc., 2018

Nomenclature

(Symbols)	(Symbol meaning)
A	magnetic vector potential
M	Magnetisation
μ	magnetic permeability
σ	electrical conductivity
N	number of turns in the coil
i	current through the coil
S	coil cross section
$u_1(t)$	voltage of coil 1
R_1	active resistances of the coil 1
R_2	active resistances of the coil 2
R_3	active resistances of the coil 3
R_4	active resistances of the coil 4
$i_1(t)$	current through the coil 1
$i_2(t)$	current through the coil 2
$i_3(t)$	current through the coil 3
$i_4(t)$	current through the coil 4
Ψ	flux linkage
T	temperature
ρ	density of the material
c	specific heat
λ	coefficient of thermal conductivity
q	volumetric density of the heat sources
h	coefficient of convection
k_B	constant of Stephan Boltzmann
ε	emissivity
T_s	temperature of the outer surface of the coils and the magnetic core
T_{amb}	ambient temperature

Journal of Energy Technology

JET Volume 14 (2021) p.p. 21-34
Issue 2, October 2021
Type of article 1.01
www.fe.um.si/en/jet.html

STATIC MODEL OF TEMPERATURE DISTRIBUTION IN A PHOTOVOLTAIC MODULE

STATIČNI MODEL TEMPERATURNE PORAZDELITVE V FOTONAPETOSTNEM MODULU

Klemen Sredenšek[1]✉, Sebastijan Seme[1,2], Gorazd Hren[1]

Keywords: photovoltaic module, temperature distribution, heat transfer, finite element method

Abstract

The primary objective of this paper is to present a static model for calculating the temperature distribution in a photovoltaic module using the finite element method. The paper presents in more detail the theoretical background of solar radiation, heat transfer, and the finite element method. The results of the static model are evaluated using temperature measurements of a photovoltaic model, which were performed at the Institute of Energy Technology, Faculty of Energy Technology, University of Maribor. The results of the regression analysis show a good concurrence between the measured and modelled values of the temperature of the photovoltaic module, especially on days with a higher share of the direct component of solar radiation.

Povzetek

Glavni cilj tega prispevka je predstavitev statičnega modela za izračun temperaturne porazdelitve v fotonapetostnem modulu po metodi končnih elementov. V prispevku je podrobneje predstavljeno teoretično ozadje sončnega sevanja, prenosa toplote in metode končnih elementov.

✉ Corresponding author: Klemen Sredenšek, M.Sc., E-mail address: klemen.sredensek@um.si

[1] University of Maribor, Faculty of Energy Technology, Hočevarjev trg 1, 8270 Krško, Slovenia

[2] University of Maribor, Faculty of Electrical Engineering and Computer Science, Koroška cesta 46, 2000 Maribor, Slovenia

Rezultati statičnega modela so ovrednoteni z meritvami temperature fotonapetostnega modela, ki so bile izvedene na Inštitutu za energetiko (Fakulteta za energetiko Univerze v Mariboru). Rezultati regresijske analize med izmerjenimi in izračunanimi vrednostmi temperature fotonapetostnega modula prikazujejo dobro ujemanje predvsem v dnevih z večjim deležem neposredne komponente sončnega sevanja.

1 INTRODUCTION

The efficiency of converting solar energy into electricity of today's photovoltaic (PV) modules ranges between 14-21 %, which means that about 80% of the solar radiation that reaches the surface of PV modules is converted into heat losses or reflected into the environment. In addition to the aforementioned, the efficiency of converting solar energy into electricity depends mainly on materials, optical losses, and other meteorological parameters. As a result, raising the temperature of a PV module significantly reduces its efficiency [1]. To this end, researchers began to develop various cooling systems that would lower the temperature of PV modules and consequently increase their efficiency [2-4]. In order to calculate the temperature of a PV module, various static mathematical models have been developed, which accurately determine the temperature of a PV module by means of correlations between heat transfer mechanisms and meteorological parameters. The simplest and most commercially used way to calculate the temperature distribution in a PV module is the Nominal Operating Cell Temperature (NOCT) model. In addition to the solar radiation and ambient temperature, all other parameters are normalised to the standard test conditions (STC) of the PV module specified by the manufacturer of the PV module. In addition to the NOCT model, a model called SNL or Sandia (Sandia National Laboratories) is also used to calculate the temperature distribution in the PV module with additional consideration of the wind speed. Due to the simplified use, the results of both models can deviate by up to 20 °C compared to the measurements of the operating temperature of PV modules [5]. In general, most of the aforementioned models are based on a state of dynamic equilibrium, which assumes that the temperature of PV modules responds instantly to atmospheric conditions. However, the conditions in the atmosphere are very dynamic and change rapidly. On this basis, dynamic models with concentrated parameters were developed [6,7], which represent greater accuracy while addressing the uniform temperature distribution through the layers of PV modules. In addition to the aforementioned dynamic models, static models with concentrated parameters [8] or numerical models (discrete methods) can also be used for accurate calculation. As mentioned above, the optical losses and electricity production of PV modules must also be considered in order to obtain an accurate calculation. In their research, specific authors [9-13] developed so-called dynamic and static thermo-electric models, which determine the operating temperature of PV modules and the production of electricity. However, it is necessary to provide enough accurate measurements to respond to a dynamic or static model [13]. For this purpose, measurement data from the year of installation of the measuring equipment were used to reduce the error between the measured and modelled results.

This paper consists of four sections. The first section provides an introduction to the research topic. The second section describes the methodology of solar radiation, heat transfer, and the finite element method, while the third section presents the results of the static model and the validation with measurements. The fourth and final section discusses the conclusions of the paper.

2 MATERIALS AND METHODS

2.1 Solar radiation

The electromagnetic waves of the Sun's rays present the power density of solar radiation that the Earth receives per unit area. Solar radiation is basically divided into direct radiation, diffuse radiation of the sky (scattered radiation), and reflected radiation (radiation reflecting off the surroundings and falling on the observed surface). In the conversion of solar energy into electrical or thermal energy, the most important contribution is direct radiation and, to a lesser extent, the contribution of diffuse and reflected radiation. To correctly determine the solar radiation on the observed surface (at a specific inclination and orientation angle), it is necessary to take into account the geometric relations between the Sun and the Earth, such as latitude (L), longitude (l), declination angles (δ), hourly angle of the Sun (ω), zenith angle (z), solar altitude angle (α_s), the azimuth angle of the Sun (γ_s), inclination angle (β), orientation angle (γ) and angle of incidence of the Sun's rays (i). Using the aforementioned parameters and some specific models [14-16], solar radiation can be predicted for any inclination and orientation angle, given by (2.1).

$$G_t(t) = G_b(t) \cdot \left(\frac{\cos(i(t))}{\sin(\alpha_s)} \right) + G_d(t) \cdot \left(\frac{1+\cos(\beta(t))}{2} \right) + G_h(t) \cdot \left(\frac{(1-\cos(\beta(t)) \cdot \rho_r)}{2} \right) \tag{2.1}$$

$G_t(t)$, $G_b(t)$, $G_d(t)$, and $G_h(t)$ are total, direct, diffuse, and global solar radiation, while the reflection factor ρ_r varies from 0 to 1, depending on the different types of surface substrates.

2.2 Heat transfer

Heat transfer deals with all the processes in which energy is transferred due to temperature differences between bodies or in matter. Heat transfer plays a vital role in many technological processes, such as accelerating heat transfer in heating or limiting heat transfer in cooling. Heat transfer can basically be divided into three mechanisms: conduction, convection, and radiation [17].

Conduction is the diffuse transport of thermal energy, in which the constituent particles of matter (atoms, molecules, electrons, and ions) rotate, vibrate, and move in a straight line. The corresponding kinetic energy increases with increasing temperature, with the kinetic energy being transferred from the higher temperature to the lower temperature range. The conduction in the case of the PV module is due to the thermal gradients between the different layers of the PV module. Fourier established a connection called the Fourier Law for one-dimensional heat transfer, which is given by (2.2), where λ is the thermal conductivity of the material.

$$q = -\lambda \frac{dT}{dx} \quad \text{oz.} \quad q(x) = -\lambda \nabla T(x) \tag{2.2}$$

The negative sign in (2) tells us that heat is transferred from the area with the higher temperature to the area with the lower temperature [17].

Convection presents a mechanism of heat transfer through the movement of a liquid or gas. In the event that the original stationary liquid is in contact with a warmer surface, its density decreases and begins to rise due to buoyancy. Such a phenomenon is called natural convection, given by (2.3), where A is the wall surface area, T_s is the wall temperature, T_f is the fluid temperature, and δ is the boundary layer thickness.

$$\phi = \lambda A \frac{T_s - T_f}{\delta} \tag{2.3}$$

Given that the wall thickness cannot be measured separately from the thermal conductivity λ, the convective heat transfer coefficient α was introduced, where the basic convection equation is given by (2.4) [17].

$$q = \alpha\left(T_s - T_f\right) \tag{2.4}$$

The convective heat transfer coefficient α was first proposed for vertical surfaces (0.5 x 0.5m) in 1924 and is still the most used equation today, involving liquid/gas velocity (given by (2.5)).

$$\alpha = 5.7 + 3.8\, v \tag{2.5}$$

Heat transfer by **radiation** differs from conductive and convective heat transfer, firstly due to the possibility of transfer through empty space and secondly due to the transfer of the proportionality of heat to the fourth exponent. The primary connection for the radiant heat flux from an optically grey surface is Stefan-Boltzmann's Law given by (2.6), where T is the body surface temperature, ε is the emissivity of the body surface, and σ is the Stefan-Boltzmann constant.

$$q = \sigma\, \varepsilon\, T^4 \tag{2.6}$$

2.3 Fourier partial differential equation for steady-state heat transfer

In the previous subsection, three basic heat transfer mechanisms were presented, which allow the heat flux to be determined at each point. For this reason, a partial differential equation (PDE) is given, representing the internal body temperature. Imagine a small cube of volume $dV = dx\, dy\, dz$, presented as part of a three-dimensional body in Figure 1. Under the influence of the temperature distribution $T(x)$ inside the body, heat flows q_k and q_{k+dk} ($k = x, y, z$) occur through six surfaces of the cube. Using the first-order Taylor approximation given in (2.7), the following heat transfer equations of the cube can be expressed from (2.8) to (2.10).

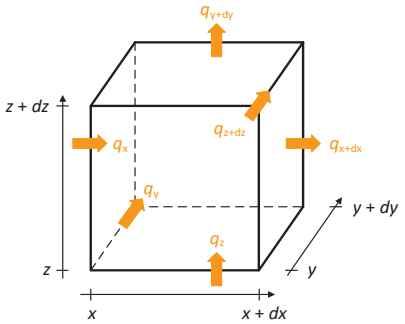

Figure 1: *A cube with volume dV and heat flows through surfaces.*

$$q_{k+dk} = q_k + \frac{\partial q_k}{\partial k} dk \quad (k = x, y, z) \tag{2.7}$$

$$\text{along the } x\text{-}axis: \left(q_x - q_{x+dx}\right) dydz = -\left(\frac{\partial q_x}{\partial x}\right) dxdydz = -\left(\frac{\partial q_x}{\partial x}\right) dV \tag{2.8}$$

$$\text{along the } y\text{-}axis: \left(q_y - q_{y+dy}\right) dxdz = -\left(\frac{\partial q_y}{\partial y}\right) dydxdz = -\left(\frac{\partial q_y}{\partial y}\right) dV \tag{2.9}$$

$$\text{along the } z\text{-}axis: \left(q_z - q_{z+dz}\right) dxdy = -\left(\frac{\partial q_z}{\partial z}\right) dzdxdy = -\left(\frac{\partial q_z}{\partial z}\right) dV \tag{2.10}$$

2.4 Finite element method

The finite element method (FEM) is used to predict mechanical, thermal, and electromagnetic systems. The FEM analysis consists of domain discretisation into finite elements, formulation of system equations, and graphical presentation. Based on the PDE given by (2.7), the boundary conditions can be determined, classified into three groups in heat transfer: Dirichlet, Neumann, and Cauchy boundary conditions.

Dirichlet boundary conditions (first type) are given by (2.11) and determine the temperature T_s at the domain/body boundary:

$$T(x,t) = T_s(x,t) \tag{2.11}$$

Neumann boundary conditions (second type) are given by (2.12) and determine the partial temperature discharge according to Fourier's Law concerning the vector n in the event of heat flux q_s from the domain/body (perpendicular to the body) [18].

$$q_s(x,t) = -\lambda \frac{\partial T}{\partial n}(x,t) \;\Rightarrow\; \frac{\partial T}{\partial n}(x,t) = -\frac{q_s(x,t)}{\lambda} \tag{2.12}$$

Cauchy boundary conditions (third type): A thermal iteration occurs between the body and the T_f fluid (shown in Figure 2). To quantify this, the body's boundaries represent the 'control volume' for an energy balance. As the thickness of the boundaries is zero, no energy can be stored within, which means that all the heat that enters the body (via conduction) must also leave the body (via convection). Cauchy boundary conditions are given by (2.13):

$$-\lambda \frac{\partial T}{\partial n}(x,t) = \alpha\left(T(x,t) - T_f\right) \tag{2.13}$$

3 RESULTS AND DISCUSSION

This section is divided into three subsections. The first subsection describes the experimental set-up of dual-axis PV tracking systems and measurement equipment, while the second

describes the model set-up performed in Ansys Transient Thermal software. The last subsection covers the validation of the model with measurements.

3.1 Experimental set-up

The input parameters of the static thermal model are various measurements performed in the experimental field of dual-axis PV tracking systems set at the Institute of Energy Technology, Faculty of Energy Technology, University of Maribor. In addition to the basic components of the PV system, dual-axis PV tracking systems also consist of several measuring devices, such as pyranometers, anemometers, and sensors for measuring the ambient temperature and the temperature of the PV module (in the center of the PV module), shown in figure 2. The PV system consists of 20 PV modules from the manufacturer PV Future with a nominal power of 260 W_p, and a total installed power of 5.2 kW_p [19]. The sampling time of the measurements is 30 min.

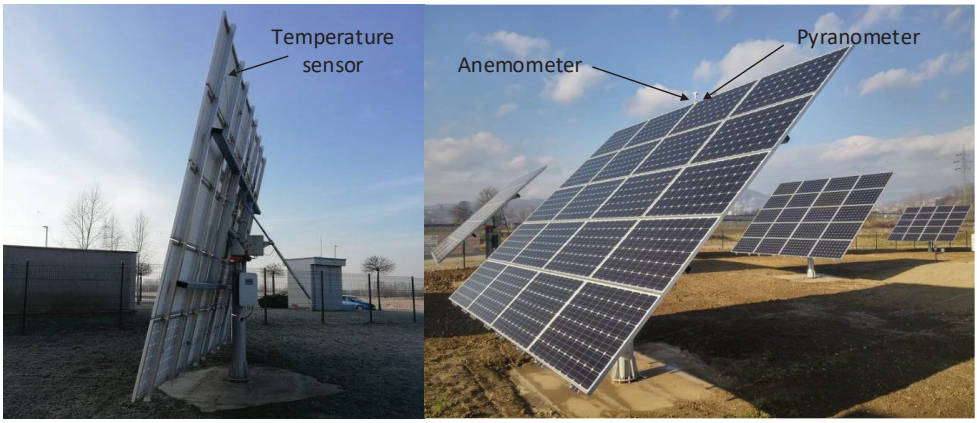

Figure 2: *Experimental set-up: Dual-axis PV tracking system equipped with measuring devices.*

3.2 Model set-up

The aim of the model is to analyse the temperature distribution on the rear of the PV module. Therefore, the model set-up performed in the Ansys Transient Thermal software is presented in detail below. A non-stationary analysis (depending on time) of heat transfer through the PV module was performed based on ambient temperature and wind speed measurements. The 3D model of the PV module was created in the Solidworks software package and imported into the Ansys Workbench software package. This was followed by determining the properties of the materials and discretising the model or dividing the geometry of the model into a finite number of small elements. Considering that the observed point was on the rear of the PV module, or more precisely at the location of the temperature measuring sensor, the model was simplified due to the calculation speed (removing the PV module's aluminum frame). The model grid was

automatically generated due to the simple geometry, using hexahedral elements as shown in Figure 3. The mesh of the model consists of 5,250 elements and 38,440 nodes.

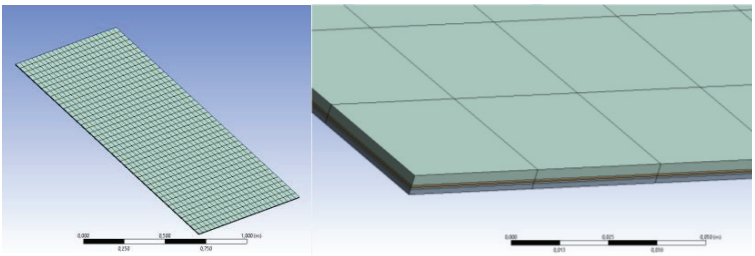

Figure 3: *Discretisation of the model.*

The PV module consists of protective glass, EVA foil, PV cells (monocrystalline silicon), EVA foil, and PolyVinyl Fluoride foil (PVF - Tedlar), as shown in Figure 4. The properties of the described materials were determined as constant values since temperatures of the PV module do not drastically affect the changes in the parameters. The thermal parameters of the materials used in the considered PV module are shown in Table 1.

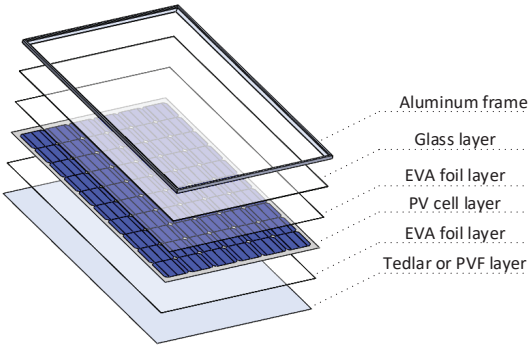

Figure 4: *Composition of the PV module by layers.*

Table 1: *Thermal parameters of the materials used in the PV module (based on the literature [9,11,13])*

	C **[J/kgK]**	***k*** **[W/mK]**	***d*** **[mm]**	***ρ*** **[kg/m^3]**
Glass	500	1.8	4	3000
EVA foil	2090	0.35	0.4	960
PV cell	677	148	0.3	2330
PVF foil	1250	0.2	0.4	1200

The boundary conditions applicable to heat transfer were subsequently defined for the PV module. As described in subsections 2.2 and 2.4, heat transfer is divided into three mechanisms: convection, conduction, and radiation. The first boundary condition involved determining the direction and magnitude of heat flux to the surface of the PV module (glass), while the second boundary condition included all other surfaces of the PV module that are subject to ambient temperature and velocity and wind direction to the surface. The determination of the boundary conditions for convection and heat flux is shown in Figure 5.

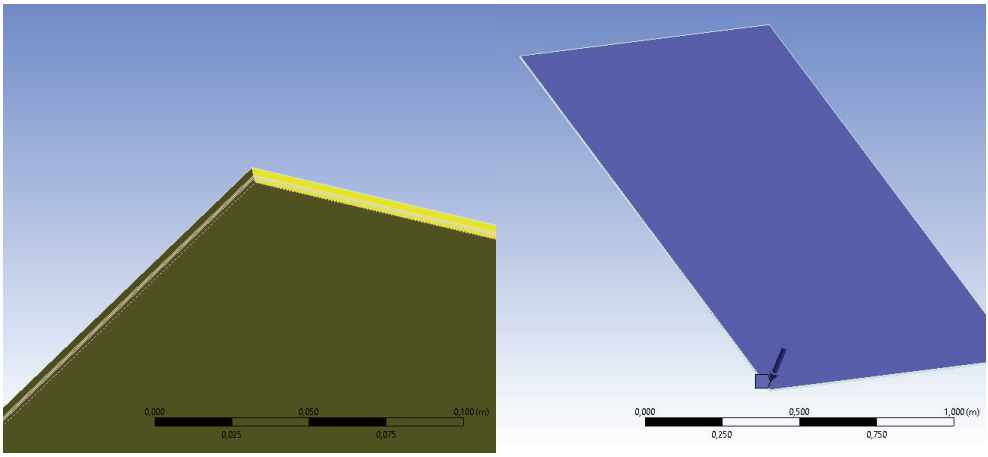

a) b)

Figure 5: *Determination of the boundary conditions – a) convection and b) heat flux.*

3.3 Validation of the model

This subsection presents the static model in the non-stationary or transient state and the validation of measured and modelled results. Figure 6 shows the various examples of contour displays of temperature distribution on the rear of the PV module at different input parameters.

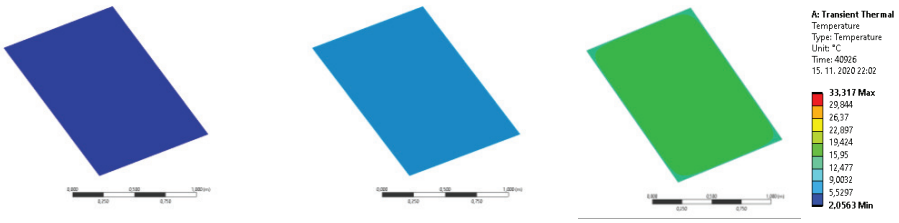

G = 46 W/m^2
α = 6,1 W/m^2°C
T_a = 3.5 °C

G = 249 W/m^2
α = 8,0 W/m^2°C
T_a = 6.4 °C

G = 579 W/m^2
α = 13,7 W/m^2°C
T_a = 8.0 °C

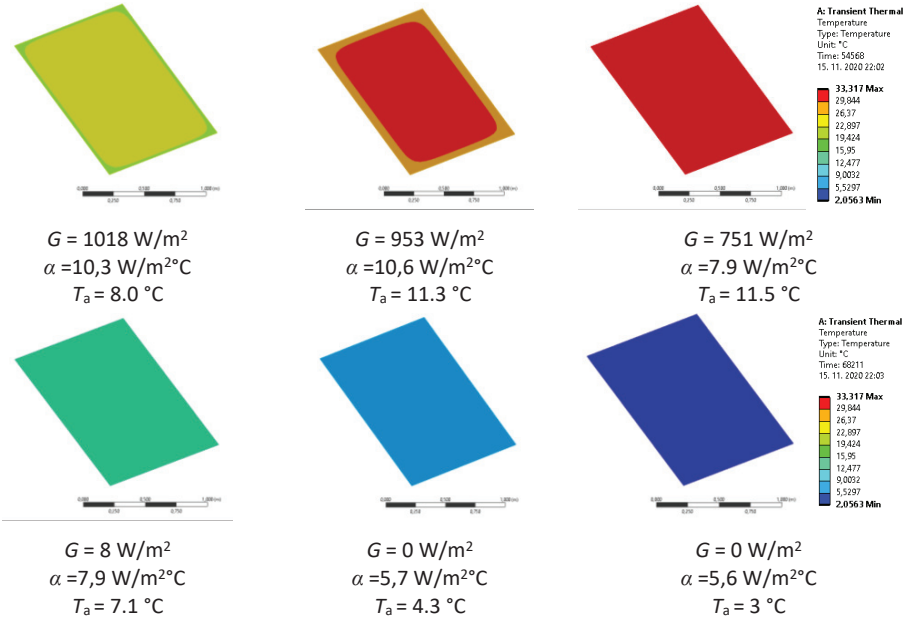

G = 1018 W/m^2
α =10,3 W/m^2°C
T_a = 8.0 °C

G = 953 W/m^2
α =10,6 W/m^2°C
T_a = 11.3 °C

G = 751 W/m^2
α =7.9 W/m^2°C
T_a = 11.5 °C

G = 8 W/m^2
α =7,9 W/m^2°C
T_a = 7.1 °C

G = 0 W/m^2
α =5,7 W/m^2°C
T_a = 4.3 °C

G = 0 W/m^2
α =5,6 W/m^2°C
T_a = 3 °C

Figure 6: *Contour display of temperature distribution at different solar radiations G, thermal transmittance coefficients α and ambient temperatures Ta.*

The three most essential parameters also presented as the boundary conditions of the static model are pre-arranged using the aforementioned equations (2.11-2.13). However, the boundary condition of heat flux (solar radiation) also considers the optical losses, which can be determined as a constant value, or as the function of the incidence angle of the Sun's rays. Figure 7 shows the validation between the measured and modelled values of the temperature distribution in the PV module for randomly selected days of the year (different weather conditions).

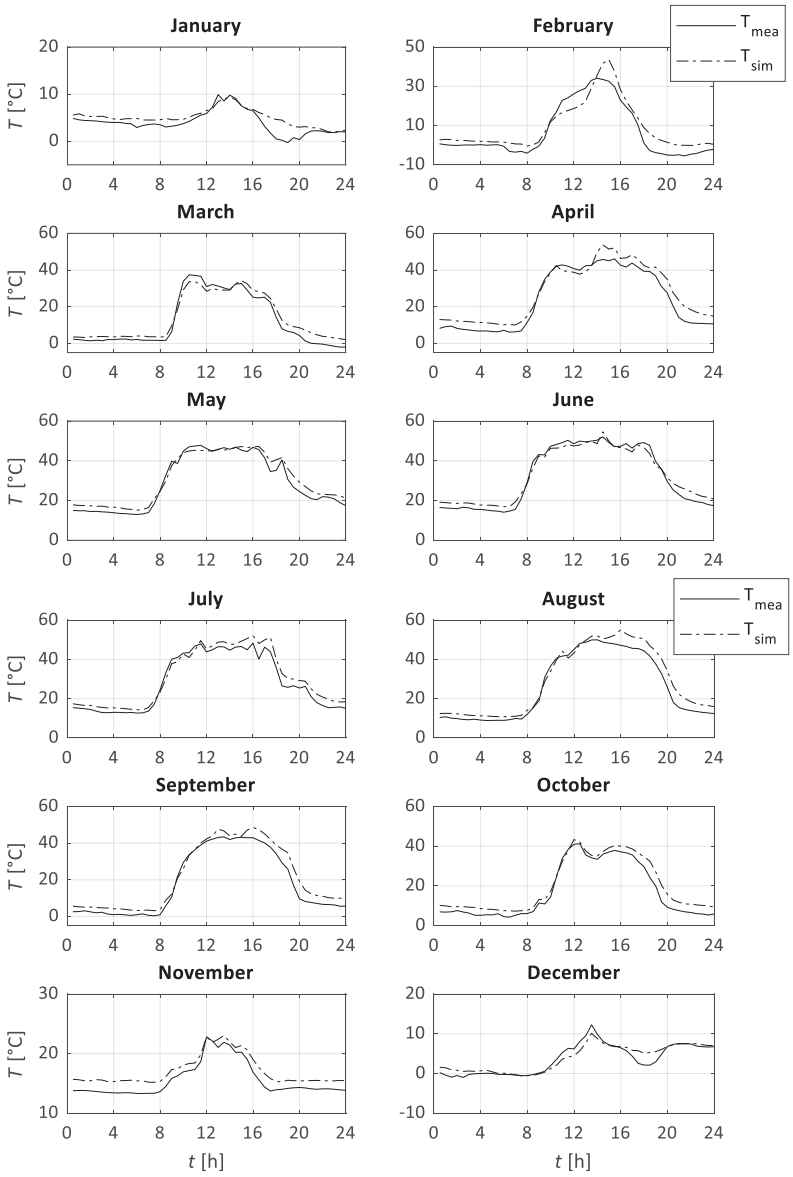

Figure 7: *Validation of the model with measurements (12 randomly selected days of the year).*

As mentioned above, the static model was performed in a non-stationary state due to easier comparison with the measurements. Figure 7 shows a slight deviation between temperatures in the summer months due to a smaller proportion of diffused solar radiation. However, the deviation in the parts without sunlight remains relatively high. In this part of the day, convection has a much more significant impact than radiation, which can be related to the measurement error of ambient temperature and wind speed.

A regression analysis was performed for a more comprehensive comparison between the measured and modelled values of the temperature distribution of the PV module. The assessment of the suitability of regression models is determined on the basis of the coefficient of determination R^2 (0 - mismatch, 1 - match).

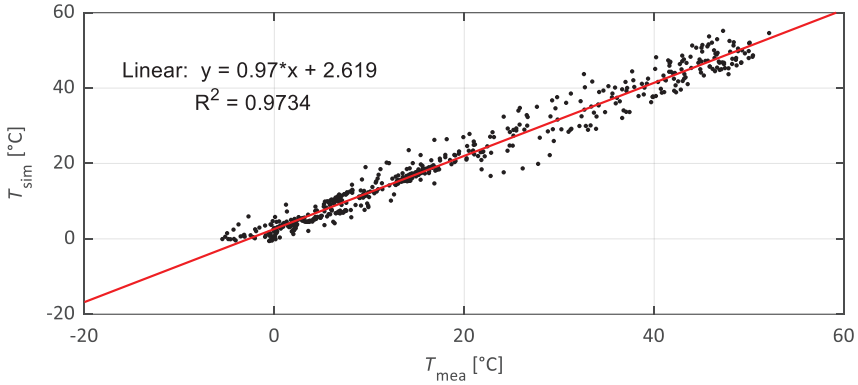

Figure 8: *Regression analysis between measured and modelled values of temperature of the PV module.*

The results in Figure 8 show a good concurrence between the measured and modelled values of the PV module temperature. It is also essential to highlight the consideration of the optical losses in the glass and PV cell layer (absorptivity, transmissivity, and reflectivity). In addition to optical losses, it is essential to consider the part of solar radiation that is converted into electricity. Since the measuring equipment does not include electrical quantities (DC voltage and DC current), it is almost impossible to determine the exact proportion of electricity.

4 CONCLUSION

This paper presents the static model of temperature distribution in a PV module performed in the Ansys Transient Thermal software package. The aim of the paper is to validate the static model of the PV module with measurements and presentation of the obtained results. The calculation of the temperature distribution in the PV module is based on measurements of solar radiation, ambient temperature, and wind speed. The static model was performed in a non-stationary state (as a function of time) and represents the change of input parameters in a half-hour time interval. The heat transfer calculation based on the static model was performed for 12 randomly selected days of the year. The results show a good concurrence between the measurements and the results of the static model. It can also be seen that more accurate results occur in the summer months due to a larger proportion of the direct solar radiation. A more significant deviation occurs in the winter months, where a higher proportion of diffuse solar radiation is present. In addition, it is essential to highlight that the regression analysis shows a larger deviation between the measurements and the results of the static model at higher temperatures and during the cooling time of the PV module.

References

[1] **H. M. Ali:** *Recent advancements in PV cooling and efficiency enhancement integrating phase change materials-based systems – A comprehensive review*, Solar Energy, Vol.197, p.p. 163-198, 2020

[2] **L. Brottier, R. Bennacer:** *Thermal performance analysis of 28 PVT solar domestic hot water installations in Western Europe*, Renewable Energy, Vol.160, p.p. 196-210, 2020

[3] **B. Widyolar, L. Jiang, J. Brinkley, S. K. Hota, J. Ferry, G. Diaz, R. Winston:** *Experimental performance of an ultra-low-cost solar photovoltaic-thermal (PVT) collector using aluminum minichannels and nonimaging optics*, Applied Energy, Vol.268, p.p. 114,894, 2020

[4] **S. Harjit:** *An Experimental comparison of two solar photovoltaic-thermal (PVT) energy conversion systems for production of heat and power*, Energy and Power, Vol.2, p.p. 46-50, 2012

[5] **B. D. Perović, D. O. Klimenta, M. D. Jevtić, M. J. Milovanovića:** *Thermal Model for Open-Rack Mounted Photovoltaic Modules Based on empirical correlations for natural and forced convection*, Thermal science, Vol.23, p.p. 3,551-3,566, 2019

[6] **C. Li, S. V. Spataru, K. Zhang, Y. Yang, H. Wei:** *A Multi-State Dynamic Thermal Model for Accurate Photovoltaic Cell Temperature Estimation*, IEEE Journal of Photovoltaics, Vol.10, No.5, p.p. 1,465-1,473, 2020

[7] **J. Barry, D. Böttcher, K. Pfeilsticker, A. Herman-Czezuch, N. Kimiaie, S. Meilinger, C. Schirrmeister, H. Deneke, J. Witthuhn, F. Gödde:** *Dynamic model of photovoltaic module temperature as a function of atmospheric conditions*, Adv. Sci. Res., Vol.17, p.p. 165-173, 2020

[8] **W.Z. Leow, Y.M. Irwan, M. Asri, M. Irwanto, A.R. Amelia, Z. Syafiqah, I. Safwati:** *Investigation of Solar Panel Performance Based on Different Wind Velocity Using ANSYS*, Indonesian Journal of Electrical Engineering and Computer Science, Vol.1, No.3, p.p. 456-463, 2016

[9] **King, D.; Boyson, W.; Kratochvil, J.:** *Photovoltaic array performance model*, Tech. Rep. 2004, p .3,535

[10] **Li, C.; Spataru, S.V.; Zhang, K.; Yang, Y.; Wei, H.:** *A Multi-State Dynamic Thermal Model for Accurate Photovoltaic Cell Temperature Estimation,* IEEE J. Photovolt., Vol.10, p.p. 1,465-1,473, 2020

[11] **Barry, J.; Böttcher, D.; Pfeilsticker, K.; Herman-Czezuch, A.; Kimiaie, N.; Meilinger, S.; Schirrmeister, C.; Deneke, H.; Witthuhn, J.; Gödde, F.:** *Dynamic model of photovoltaic module temperature as a function of atmospheric conditions,* Adv. Sci. Res., Vol.17, p.p. 165-173, 2020

[12] **Yu, Q.; Hu, M.; L.; J.; Wang, Y.; Pei, G.:** *Development of a 2D temperature-irradiance coupling model for performance characterizations of the flat-plate photovoltaic/thermal (PV/T) collector,* Ren. Ener., Vol. 153, p.p. 404-419, 2020

[13] **Sredenšek, K.; Štumberger, B.; Hadžiselimović, M.; Seme, S.; Deželak, K.:** *Experimental Validation of a Thermo-Electric Model of the Photovoltaic Module under Outdoor Conditions,* Appl. Sci., Vol.11, p. 5,287, 2021

[14] **Liu, B.Y.H., Jordan, R.C.:** *Daily insolation on surfaces tilted towards the equator,* ASHRAE JOURNAL, Vol.3, p.p. 53-59, 1961

[15] **Jimenez, J.I.:** *Effects of solar radiation on the performance of pyrometers with silicon domes*, J. Atmos. Ocean. Technol., Vol.5, p.p. 666-670, 1988

[16] Klucher, T.M.: *Evaluation of models to predict insolation on tilted surfaces,* Sol. Energy, Vol.23 (2), p.p. 111-114, 1979

[17] **B. Pentenrieder:** *Finite Element Solutions of Heat Conduction Problems in Complicated 3D Geometries Using the Multigrid Method*, Thesis, Technical University of Munich, Faculty of Mathematics, 2005

[18] **G. Gimenez, M. Errera, D. Baillis, Y. Smith, F. Pardo:** *Analysis of Dirichlet-Robin interface condition in transient conjugate heat transfer problems*, Application to a flat plate with convection 11th European Conference on Turbomachinery Fluid Dynamics and Thermodynamics - ETC 2015, MADRID, Spain, 2015

[19] **Photovoltaic modules - PVF 260.** Available online: http://www.pvfuture.eu/static/uploaded/pdf/PVF60M_SLO.pdf (accessed on 30 June 2021)

Nomenclature

(Symbols)	(Symbol meaning)
A	wall surface area
c_p	heat capacity
G_b	direct component (beam) of solar radiation
G_d	diffuse component of solar radiation
G_h	solar radiation on horizontal surface
G_t	solar radiation on tilted surface
i	Incident angle of the Sun's rays
L	length
n	vector
q	heat flux
q_s	heat flux from the body/domain
q_x	heat flux along x-axis
q_y	heat flux along y-axis
q_z	heat flux along z-axis

T	temperature
T_a	ambient temperature
T_f	fluid temperature
T_s	wall temperature
V	wind speed
V	volume
α	convective heat transfer coefficient
α_s	solar altitude angle
β	inclination angle
δ	boundary layer thickness
ε	emissivity of the body surface
λ	thermal conductivity
ρ	density
ρ_r	reflection factor
σ	Stefan-Boltzmann's constant
PV	photovoltaic
STC	standard test conditions
FEM	finite element method
EVA	ethylene-vinyl
PVF	polyvinyl fluoride

Journal of Energy Technology

JET Volume 14 (2021) p.p. 35-46
Issue 2, October 2021
Type of article 1.01
www.fe.um.si/en/jet.html

A STUDY OF PARTICULATE AND GASE-OUS EMISSIONS OF A DAMAGED TUBU-LAR COMBUSTION CHAMBER IN A PELLET STOVE

ŠTUDIJ TRDIH DELCEV IN PLINSKIH EMISIJ V POŠKODOVANI CEVNI IZGOREVALNI KOMORI PELETNE PEČI

Zdravko Praunseis[1]

Keywords: particulate matter, small scale pellet boilers, combustion chamber, fine particle emission, pellet burner

Abstract

Wood-burning boilers are a popular source of heating in Slovenia. However, there has been much debate about the potential negative health effects associated with wood smoke in recent years. Wood smoke is increasingly seen as a significant component of airborne particulate matter (PM), especially in the context of the new sort time standard for fine particles in ambient air. Most organic substances will be burnt in the boilers during good combustion conditions with sufficient oxygen supply and high temperature.

This study presents the influence of damaged tubular combustion chamber on smoke fine-particle emissions at small scale pellet burners. This research aims to reduce the particulate matter emissions of small scale pellet boilers and contribute to cleaner air.

[1] Corresponding author: Zdravko Praunseis, PhD, Associate Professor, Faculty of Energy Technology, University of Maribor, Tel.: +386 31 743 753, Fax: +386 7 6202 222,
Mailing address: Hočevarjev trg 1, Krško, Slovenia, E-mail address: zdravko.praunseis@um.si

Povzetek

Kotli na lesno biomaso so priljuljen način ogrevanja v Sloveniji. V zadnjih letih je bilo veliko govora o potencialno negativnem vplivu izgorevalnih plinov na zdravje ljudi. Glede na dovoljene vrednosti trdih delcev v zraku, ki jih predpisuje novejši standard, je postal izgorevalni plin v pečeh na lesno biomaso eden od znatnih onesnaževalcev okolja s trdimi delci. V primeru popolnega izgorevanja v pečeh pri višjih temperaturah z zadostno količino kisika, večina organskih snovi izgori.

V tej študiji je predstavljen vpliv poškodovane cevne izgorevalne komore na emisijo trdih delcev v manjših peletnih pečeh. Glavni namen raziskave je zmanjšati možnosti pojava trdih delcev v izgorevalnih plinih peletnih pečeh in s tem prispevati h čistejšemu zraku.

1 INTRODUCTION

Residential wood combustion has been identified as one of the main sources of particulate matter (PM); fine particles are significant because of their adverse effects on human health and the environment, *[1].* Particulate matter is defined as the total mass of suspended particles in the air. PM is typically divided into three subclasses, i.e., PM10, PM2.5 and PM0.1, which are defined as particle matter with an aerodynamic diameter smaller than 10 µm, 2.5 µm, and 0.1 µm, respectively. PM2.5 particles are generally called “fine particles”; however, this term can also be applied to the number or surface area based on particle diameters less than 2.5 µm. In the atmosphere, particles can be solid or liquid; the mixture of particles and gases is called an “aerosol”, *[2]*. When particles from combustion sources are discussed, particles with aerodynamic diameters less than 1 µm or 2.5 µm (PM1 or PM2.5) are often used, whereas particles with sizes ranging from 2.5 µm to 10 µm are called “coarse particles”. Examples of coarse particle sources include road wear and wind-blown dust, *[3]*. Fine particles are known to have adverse effects on human health and to cause respiratory and cardiac symptoms and even premature death, especially among those with reduced health conditions, e.g., children, the elderly, and those with chronic diseases.

Small scale combustion appliances are mainly used for residential heating in Slovenia. Different types of small-scale combustion appliances, such as wood stoves, pellet burners, pellet boilers, wood log boilers, and wood chip boilers, are commonly used throughout Europe and in Slovenia. Different forms of biomass fuels, such as wood logs, wood chips, wood pellets, sawdust, forest residues, straw, etc., are used as fuel in these appliances.

Wood is the most commonly used biomass fuel in Slovenia due to the large forest base, forest industry, and relatively easy access to cheap wood for many individuals. The use of wood in heat and power production is increasing. Wood pellets are primarily used in continuously operated combustion devices, *[4]*, as an example of renewable energy.

In this study, the influence of a damaged tubular combustion chamber on smoke fine particle emissions from pellet burners is presented. The purpose is to reduce particulate matter emissions from the small scale pellet boilers and contribute to cleaner air.

2 EXPERIMENTAL SECTION

Combustion experiments were performed in a laboratory environment with a small-scale 25 kW pellet boiler suitable for household heat production. The pellet boiler operates with an overfed fuel input and includes a Ferroli Sun P7 prefabricated burner (Figure 1). This type of pellet burner is the most popular in Slovenia due to its reasonable price. The burner can be operated continuously between loads of 14 and 30 kW. It is equipped with logic-controlled fans for the supply of combustion air. The primary air was fed in through holes before the grille at the bottom of the cylindrical furnace, i.e., a tubular combustion chamber with 3 mm steel wall thickness. The width of the grille was approximately 100 mm, and the diameter of each hole was approximately 6 mm. Commercial wood pellets originating from Slovenia were used in the study. The primary pellet raw material was pinewood.

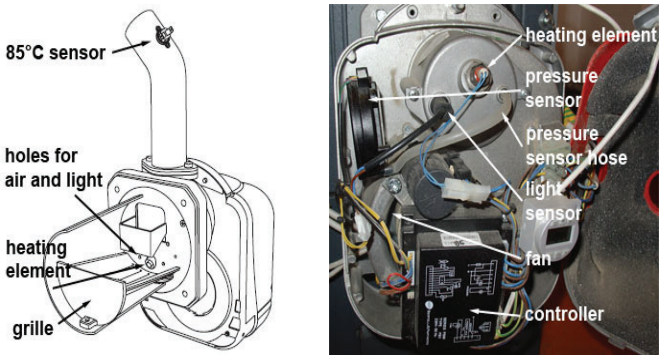

Figure 1: *Sketch of the pellet burner used in this study*

The tubular combustion chamber should be made of high-temperature-resistant steel that contains a prescribed amount of Cr and Mo due to the high flame temperature, which can exceed 600 °C (point M17). The distribution of the flame temperatures was measured with a Testo 890-2 infrared camera, as shown in Figure 2 and Table 1.

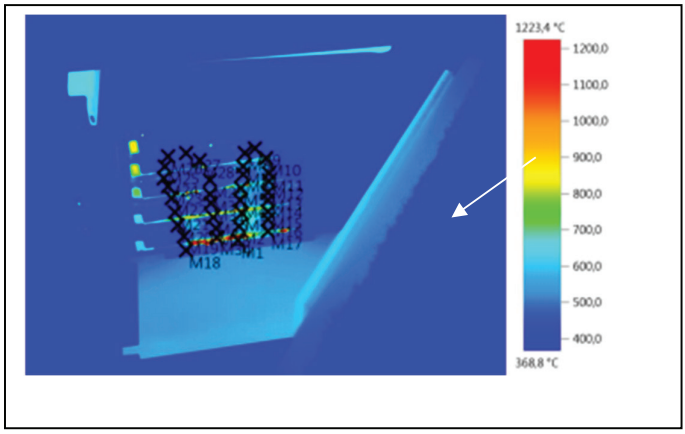

Figure 2: *Flame temperature measurement at the tubular combustion chamber of pellet burner*

Table 1: *Temperature distribution at pellet burner's flame*

Measure point	Temp. [°C]	Emiss.	Refl. Temp. [°C]
Measure point 1	573.5	0.13	20.0
Measure point 2	514.7	0.13	20.0
Measure point 3	575.8	0.13	20.0
Measure point 4	545.9	0.13	20.0
Measure point 5	513.8	0.13	20.0
Measure point 6	442.0	0.13	20.0
Measure point 7	492.7	0.13	20.0
Measure point 8	418.8	0.13	20.0
Measure point 9	394.2	0.13	20.0
Measure point 10	529.6	0.13	20.0
Measure point 11	460.4	0.13	20.0
Measure point 12	615.2	0.13	20.0
Measure point 13	460.6	0.13	20.0
Measure point 14	413.4	0.13	20.0
Measure point 15	569.8	0.13	20.0
Measure point 16	493.7	0.13	20.0
Measure point 17	643.0	0.13	20.0
Measure point 18	237.7	0.13	20.0
Measure point 19	329.2	0.13	20.0
Measure point 20	386.1	0.13	20.0
Measure point 21	348.9	0.13	20.0
Measure point 22	416.4	0.13	20.0
Measure point 23	322.1	0.13	20.0
Measure point 24	439.1	0.13	20.0
Measure point 25	302.9	0.13	20.0
Measure point 26	391.0	0.13	20.0
Measure point 27	391.2	0.13	20.0
Measure point 28	318.1	0.13	20.0

Measure point 29	327.3	0.13	20.0
Measure point 30	409.9	0.13	20.0
Measure point 31	353.3	0.13	20.0
Measure point 32	424.9	0.13	20.0
Measure point 33	390.3	0.13	20.0
Measure point 34	393.8	0.13	20.0

The shape of the pellet burner's flame can be seen in Figure 3. The arrow marks the area with the highest measured temperature (point M17), 643 ℃ (Figure 2 and Figure 3 and Figure 4).

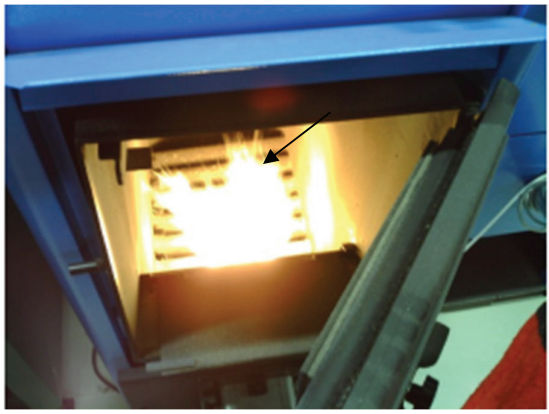

Figure 3: *The shape of the flame in the pellet burner*

The damage of the steel tube (tubular combustion chamber) and the grille occurred after one year of the burner operation time, as shown in Figure 4 and Figure 5.

Figure 4: *Hole as a damage of the steel tube (tubular combustion chamber)*

Figure 5: *Hot cracks as a damage of the steel grille*

Chemical analyses of the steel tube (tubular combustion chamber) and Cr-Mo steel tube was performed with X-ray fluorescence spectrometry (XRF) using an X-ray fluorescence spectrometer (Thermo Scientific Niton XL3t GOLD+) and is given in Table 2.

Measurements were carried out manually (Figure 6) with the target points on the steel tube (Figure 7). Each measurement was repeated three times, and later the average value was calculated. Each measurement was done for one minute.

Table 2: *Chemical composition of steel tube (tubular combustion chamber)*

(%)	C	Si	Mn	P	S	Cr	Ni	Mo	Cu	Al
HSLA Steel tube	0.17	0.57	0.71	0.021	0.004	0.49	0.08	0.028	0.31	0.027
X11CrMo9 Steel tube	0.08	0.41	0.63	O.031	0.002	8.23	0.04	0.96	-	-

The basic mechanical properties of the steel tube were obtained using flat tensile specimens taken from the steel tube in the rolling direction; they are given in Table 3.

Table 3: *Real mechanical properties of steel tube (tubular combustion chamber)*

Designation	R_p (MPa)	R_m (MPa)	Elongation (%)	Charpy toughness (J)
Steel tube	736	817	16.2	79,88,112 at 0 ℃

Figure 6: *Manual measurement of chemical analyses of steel tube (tubular combustion chamber) with X-ray fluorescence spectrometry (XRF) using an X-ray fluorescence spectrometer*

Figure 7: *Target point (number 2) for manual measurement of chemical analyses of real steel tube (tubular combustion chamber)*

Fine particle measurements were made in the chimney tube at a distance of 20 cm from the boiler using a fine particle analyser (Figure 8), which measures fine particles, O_2 concentration and CO emissions in real-time for 15 minutes.

Figure 8: *Fine particle measurement with the Testo 380 fine particle analyser*

3 RESULTS AND DISCUSSION

From the results of chemical analyses (Table 2) and real mechanical properties (Table 3) of the steel tube (tubular combustion chamber), it is evident that the high-strength, low-alloyed (HSLA) steel is used for the construction of the tubular combustion chamber. This steel is typically HSLA carbon steel, with a comparatively mild amount of carbon (0.16% to 0.20%) and a low amount of Cr and Mo, which is less than 0.5% (Table 2). It has ferromagnetic properties. The mild amount of carbon also makes HSLA steel vulnerable to rust. HSLA steel is used in construction as structural steel and is not useful for operation at temperatures higher than 100 ℃ due to the low content of Cr and Mo, as can be seen from Table 2. The characteristic fine-grain bainitic microstructure of the HSLA steel tube is shown in Figure 9. The surface of a metallographic specimen is prepared by polishing and etching. After preparation, it is analysed using a Zeiss Axio A2 optical microscope.

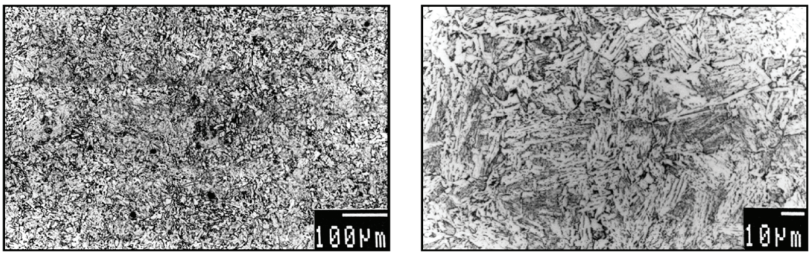

Figure 9: *The characteristic fine-grain bainitic microstructure of a real HSLA steel tube*

The tubular combustion chamber should be made from high-temperature Cr-Mo resistance steel, which contains a prescribed amount of Cr (at least 9%) and Mo (about 1%) due to the high flame temperature, which can exceed 600 ℃. The improper selection of base material (HSLA steel) leads to the damage of the steel tube due to the high operating temperatures during the combustion of pellets (Figure 4). The highest flame temperature of 643 ℃ (Figure 2, point M17, see arrow) was measured at the surface of the HSLA steel tube end (Figure 3 and Figure 4, see arrow) with an

infrared camera, as shown in Figure 2 and Table 1. Thus, the tubular combustion chamber must be made from a high-temperature Cr-Mo steel, containing a prescribed amount of Cr and Mo.

The damage appeared at the burner tube as holes, as can be seen from Figure 4. The total measured amount of damaged tube surface was 22.75 cm².

Because of this, holes with diameters of 11 mm were drilled into the new steel tube (Figure 10 and Figure 11) made of X11CrMo9 high-temperature-resistant steel to simulate the damage of the tube (tubular combustion chamber) measured with a fine particle analyser (Figure 8).

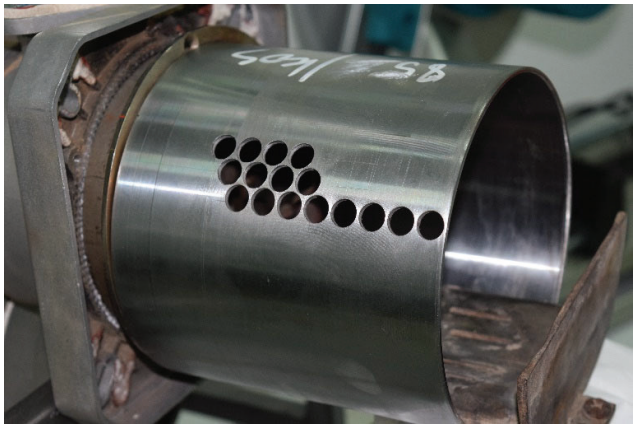

Figure 10: *Cr-Mo steel tube with damaged surface (16 holes)*

Combustion experiments were performed with optimal operational manipulation (loads, primary combustion air supplies). Normal operation was assumed to obtain a nominal load of 25 kW, represented as an optimal baseline.

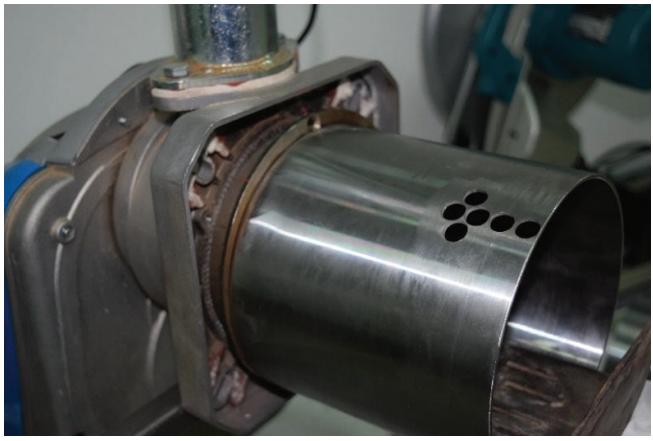

Figure 11: *Cr-Mo steel tube with damaged surface (6 holes) of 5.70 cm²*

Each of the combustion experiments was performed in a preheated pellet boiler. The boiler was turned on one hour before the start of the experiment, and the warming was performed on full load.

The influence of damaged tubular combustion chamber on smoke fine-particle emissions (FPE), O_2 concentration, and CO emissions at the pellet burner is presented in Table 4 and Figure 12. Table 4 presents the total values of smoke fine-particle emissions (FPE), O_2 concentration and CO emissions after 15 minutes of measurements with the fine particle analyser.

By reviewing the results (Table 4 and Figure 12) of measurements of smoke fine-particle emissions (FPE), O_2 concentration and CO emissions, it is clear that the highest values were reached at the largest damaged tube surface at 22.75 cm^2 (24 holes). FPE value is approximately 77% higher than the optimal value at the zero damage surface. The damaged combustion chamber of the pellet burner influences lower O_2 concentration for about 48% and approximately 50% higher CO emissions in comparison with optimal values at the zero damage tube surface.

Table 4: *The results of measurements of smoke fine-particle emissions (FPE), O2 concentration and CO emissions at the damaged pellet burner chamber*

Damage surface (cm^2)	**FPE (mg/Nm^3)**	**O_2 (%)**	**CO (mg/Nm^3)**
0.00	16.7	6.2	68
0.95 (1 hole)	16.9	6.1	69
1.90 (2 holes)	17.1	5.8	72
3.80 (4 holes)	17.9	5.1	75
5.70 (6 holes)	18.1	4.9	79
22.75(24 holes)	29.6	3.2	101

The damage effect of the tubular combustion chamber on smoke fine-particle emissions (FPE), O2 concentration and CO emissions is insignificant at damage surfaces 0.00 cm^2, 0.95 cm^2, 1.90 cm^2, and 3.80 cm^2 (4 holes) for which the measured values did not exceed 7% of optimal values.

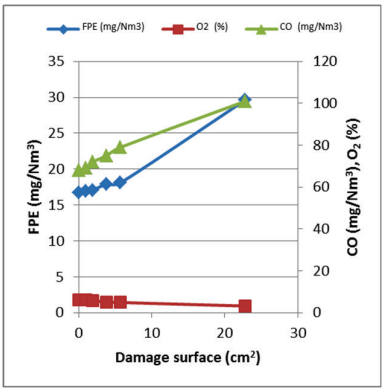

Figure 12: *The influence of damaged tubular combustion chamber on smoke fine-particle emissions (FPE), O_2 concentration and CO emissions at the pellet burner*

The next higher values were reached at the damaged tube surface of 5.70 cm² (6 holes). FPE value is approximately 10% higher than the optimal value at the zero damage surface. The damaged pellet burner chamber also influenced lower O_2 concentration by about 20% and approximately 13% higher CO emissions in comparison with optimal values at the zero damage tube surface.

4 CONCLUSION

Wood is the most commonly used biomass fuel in Slovenia due to the large forest base, forest industry, and relatively easy access to cheap wood for many individuals. The use of wood in heat and power production is increasing. Wood pellets are primarily used in continuously operated combustion appliances. In real applications, combustion conditions are never ideal. Moreover, fuel and combustion air contain several components that affect the combustion process and emission formation. The combustion of solid fuel in real-life applications always require more air than what is theoretically needed.

The tubular combustion chamber of a pellet burner should be made from high-temperature-resistant Cr-Mo steel that contains prescribed amounts of Cr and Mo due to the high flame temperature, which can exceed 600 °C.

Improper selection of base materials for the construction of steel combustion tubes leads to damage due to the high operating temperatures during the combustion of pellets.

The damage appeared on the burner tube as holes. A damaged tubular combustion chamber in the pellet burner significantly influences smoke fine-particle emissions (FPE), O_2 concentrations, and CO emissions.

The highest values of smoke fine-particle emissions (FPE), O_2 concentration, and CO emissions were reached at the largest damaged tube surface: 22.75 cm² (24 holes). The FPE value is approximately 77% higher than the optimal value on the non-damaged surface. A damaged pellet burner chamber also influences lower O_2 concentration by about 48% and approximately 50% higher CO emissions in comparison with optimal values at the zero damage tube surface. The damage effect of the tubular combustion chamber on smoke fine-particle emissions (FPE), O_2 concentrations, and CO emissions is insignificant at damage surfaces 0.00 cm², 0.95 cm², 1.90 cm² and 3.80 cm² (4 holes) for which measured values did not exceed 7% of optimal values.

Pellet boilers save energy and money, and they are highly durable; however, regular maintenance, especially of the tubular combustion chambers, is essential to keep them working efficiently and contributing to cleaner air.

Acknowledgements
The authors thank the firm Žaga Cugmajster d.o.o. Loče, Slovenia for the pellet material supply.

References

[1] **Z. Praunseis and R. Strojko:** *Energy supply of buildings*, University Handbook, Krško: University of Maribor, 2013

[2] **Z. Praunseis and R. Strojko**: *Energy renovation of an older house*, Science journal of energy engineering, vol. 2, pp. 47-52, Aug. 2014

[3] **H. Lamberg:** *Physicochemical properties of fine particles from small-scale wood combustion*, *Atmospheric Environment*, vol. 45, pp. 7635–7643, Feb. 2011

[4] **U. Fernandes and A. Costa:** *Formation of fine particulate matter in a domestic pellet-fired boiler*, Energy & Fuels, vol 27, pp. 1081–1092, Jan. 2013

Journal of Energy Technology

JET Volume 14 (2021) p.p. 47-55
Issue 2, October 2021
Type of article 1.01
www.fe.um.si/en/jet.html

GEOMETRY DESIGN AND ANALYSIS OF AN ELECTRIC BUS FOR THE INTERIOR THER-MAL MODELLING

DIZAJNIRANJE IN ANALIZA TERMIČNEGA MODELIRANJA NOTRANJOSTI ELEKTRIČ-NEGA AVTOBUSA

Costică Nițucă[1], Gabriel Chiriac[1✉], Georgel Gabor[1], Ilie Nucă[2], Vadim Cazac[2], Marcel Burduniuc[2,]

Keywords: heat transfer, electric bus, passenger comfort, geometry design, thermal modelling

Abstract

The heating, ventilation and air-conditioning (HVAC) system represents the main auxiliary load for any type of bus. Being the most significant energy-consuming auxiliary load for the electric bus, it must be given special attention in an electric bus system design. To study the heat transfer and thermal optimization for passenger comfort in the electric bus computer-aided design (CAD) is used. The geometry of an electric bus interior is designed considering the main components of the vehicle: passenger cabin, driver's cabin, windows, walls, and seats. Materials of the same type as those used in the real bus are considered for the geometry model. Based on the heat transfer theory, a thermal model and simulations are made for the heat transfer inside the electric bus. The simulated data are compared with measurement data, and based on these, it can be concluded that the thermal model of the electric bus can be validated and used further for a wide variety of thermal simulation types.

✉ Corresponding author: Lecturer Ph.D., Chiriac Gabriel, Tel.: +040 727 645058, Mailing address: Bd. Prof. Dimitrie Mangeron, nr. 21-23, 700050 Iasi, Romania, E-mail address: gchiriac@tuiasi.ro

[1] "Gheorghe Asachi" Technical University from Iasi, Faculty of Electrical Engineering, Romania

[2] Technical University of Moldova, Chisinau, Faculty of Power and Electrical Engineering, Republic of Moldova

Povzetek

Sistem ogrevanja, prezračevanja in klimatizacije (HVAC) predstavlja glavno dodatno obremenitev za vse vrste avtobusov. Ker gre za sistem z največjo porabo energije pri električnem avtobusu, mu moramo posvetiti posebno pozornost pri dizajniranju električnega avtobusa. Pri študiji prenosa toplote in optimizaciji v smislu udobja potnikov smo uporabili računalniško podprto dizajniranje (CAD). Postavitev notranjosti električnega avtobusa je zasnovana glede na glavne komponente vozila: prostor za potnike, prostor za voznika, okna, stene in sedeže. V oblikovanem modelu so uporabljeni materiali iste vrste kot v realnih avtobusih. Na podlagi teorije o prenosu toplote smo naredili model in simulacije prenosa toplote znotraj električnega avtobusa, nakar smo primerjali podatke iz simulacije s podatki iz meritev. Iz izvlečkov omenjene primerjave lahko zaključimo, da je termični model električnega avtobusa mogoče validirati in nadalje uporabiti za najrazličnejše termične simulacije.

1 INTRODUCTION

Energy consumption per trip for an urban vehicle is a major design factor, which is influenced by the driving pattern, the topology, the climate conditions and the payload. The energy required by the auxiliaries is not negligible, so that the efficiency enhancement of the auxiliaries could lead to an improvement of global energy use in the vehicle, which is particularly important for innovative means of transport which are characterised by a limited range, such as that of an electric bus.

The importance of energy consumption for non-traction needs is revealed when considering the percentage distribution of energy consumption in annual scales for a bus system *[1]*: traction needs represent about 52%, non-traction needs on stopping about 13% and non-traction needs for route operation about 35%.

A key parameter affecting the auxiliary energy consumption is the external temperature. A rise of 10 ^{o}C can lead to an energy consumption increase of about 0.75kWh/km *[2]*.

An important input parameter is the setpoint temperature within the electric bus cabin. Usually, the setpoint is kept at a constant temperature that is comfortable for the passengers inside the bus, but the “comfort aspect” is a relative aspect concept. What a person perceives as a comfortable temperature depends on many parameters, such as *[3]* air humidity, air velocity, radiation, seasonal effects, and metabolism.

Attention is given to the optimization of the thermal system of electric vehicles. This functionality can be synthesized as:

1. Dynamic temperature setpoint: By considering the different aspects of comfort, an energy-optimized temperature setpoint control can be implemented. For example, a temperature setpoint can vary over the day to account for ambient temperature changes. This results in lower energy consumption of the HVAC system *[3]*.

2. Pre-conditioning: The energy that is required for the heat to control the cabin climate is taken from the battery. Therefore, this might affect the driving range of the vehicle. Besides minimizing the energy consumption of the HVAC system, pre-conditioning can also be applied to improve the vehicle’s driving range of the vehicle. Pre-conditioning means that the cabin

climate is already controlled towards the desired temperature while the vehicle is still connected to the charger, either in the depot or en route at terminal stops.

Heat transfer theory, heat balance method and U-Value definition are the foundations used in calculations and modelling *[4]*. Based on the heat transfer theory, there are three mechanisms for transferring heat: conduction, convection and radiation.

The Heat Balance Method is a common method for calculation of heating and cooling loads in a space or zone *[4]*. The total heat released into the cabin is given by:

- Ambient load, as the thermal load caused by the temperature gradient between inside air and the ambient temperature,
- Radiation loads,
- Metabolic load, generated by human body,
- Ventilation load, as the flow of fresh air,
- Engine/Motor load, due to the bus motors,
- AC load, for keeping the internal temperature in the comfort zone by heating or cooling.

The heating, ventilation and air-conditioning (HVAC) system represents the main auxiliary load for any type of bus. Being the most significant energy-consuming auxiliary load for the electric bus, it must be given special attention in an electric bus system design. The HVAC systems usually implemented in electric buses is composed from a rooftop unit comprising a compression refrigeration machine and several heat exchangers for air cooling and heating. Heating can be also performed by heaters placed at the floor level and supplied from the main power supply, or from an auxiliary supply system (such as a battery), *[5-8]*.

Energy needs for resistance heating can significantly increase the vehicle's energy consumption. From measurements on a 12 m electric bus *[9]*, it is estimated the average electric power necessary to keep the interior of the vehicle at 17 ^{o}C on a cold winter day with ambient temperature of approximately -10 ^{o}C is around 24 kW. Assuming a specific energy demand for traction and non-HVAC auxiliaries of 1.2 kWh/km, a plausible value according to measurements, a constant 24 kW load for heating will increase vehicle consumption by 1.3 kWh/km at an average velocity of 18 km/h and 2 kWh/km at an average velocity of 12 km/h.

Possible measures to reduce energy consumption of the HVAC system include improved thermal insulation, double-glazed windows, door air curtains and using improved control systems. Differently from the conventional HVAC system on current buses, *[10]* an integrated air-conditioning and heating system specifically for an electric bus are proposed. For an i-HVAC (integrated HVAC) system, an electrical heat pump type should be considered.

2 HEAT TRANSFER MODEL

Thermal conduction is estimated considering Fourier's Law, with heat flux given by:

$$q=-k\cdot dT/dx \ [W/m2] \quad (2.1)$$

where:

q is the heat flux,

k is the thermal conductivity, [W/m^2K],

T is temperature, [^oC],

x direction of the heat flux, [m].

Thermal convection is considered for the heat transfer between the air and the solid structure of the bus. Newton's formula is considered in this case for the heat flux estimation:

$$q=-h\cdot(T_s-T_f) \ [W/m2] \quad (2.2)$$

where:

q is the heat flux,

h heat transfer coefficient, [W/m^2K],

T_s is the temperature of the solid, [^oC],

T_f is the temperature of the fluid, [^oC].

3 DESIGNING THE INTERIOR GEOMETRY MODEL OF THE ELECTRIC BUS

To study the heat transfer and thermal optimization for passenger comfort in the electric bus, computer-aided design (CAD) is used, COMSOL Multiphysics, which has a special application for thermal aspects, the Heat Transfer Module. In order to simulate the heat process inside the bus, the following steps are to be followed: geometry modelling, physics settings, solving, and results.

The geometry of the electric bus is constructed as a basic geometry and is composed from: passenger cabin; driver's cabin; bus walls; windshield; windows; floor; roof; doors; wheels; passengers seats; electric air heat units inside the passenger cabin; heating block inside the driver's cabin.

The dimensions of the electric bus are designed in the geometry model according to the actual dimensions of the real vehicle, an E321 electric bus used currently in public transportation in Chisinau, Republic of Moldova *[11, 12]*. This is a low-floor compartment vehicle with a capacity of about 100 passengers, with a 150kW electric motor, with four heating units inside the passenger cabin. The components of the vehicle described above are also designed on the geometry model considering their actual dimensions on the electric bus. Thus, the model and the simulation results will be close to reality.

The first step to build the geometry model of the electric bus was to design the passengers' cabin and the driver's cabin. For the modelling and simulations these areas will be considered to be filled with air.

The second step in designing the geometry model is to design the exterior components, such as the front wall, rear wall, lateral walls, front windows (windshield), rear window, lateral windows and the doors. For this, a 2D representation was used (Figure 1), as a work plane design and plane geometry design. For each of these components, coordinates for the size, shape and position are transferred into the geometry model.

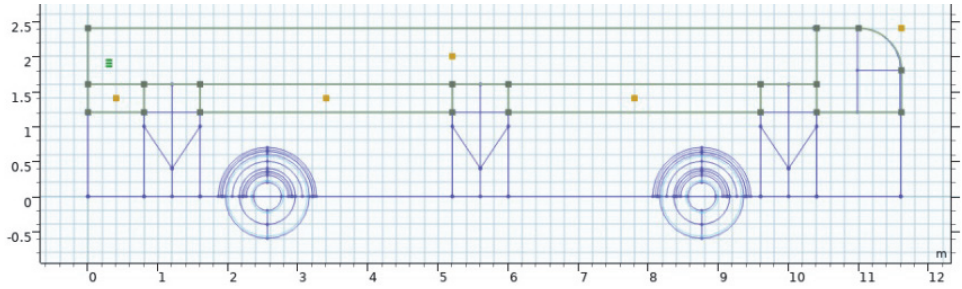

Figure 1: *2D design of the bus*

Having the main structure of the geometry model, the heaters can be designed inside the cabins. The passenger cabin is designed with four heaters and the driver's cabin with one heater (Figure 2). Thus, in the passenger cabin, the first heater is placed on the right side of the vehicle, next to the third door, a second heater is placed on the left side of the vehicle, in the middle area, the third heater is placed on the right side, after the second door, and the fourth heater is placed in front of the cabin, next to the glazed partition which separates the driver's cabin from the passenger compartment (Figure 2).

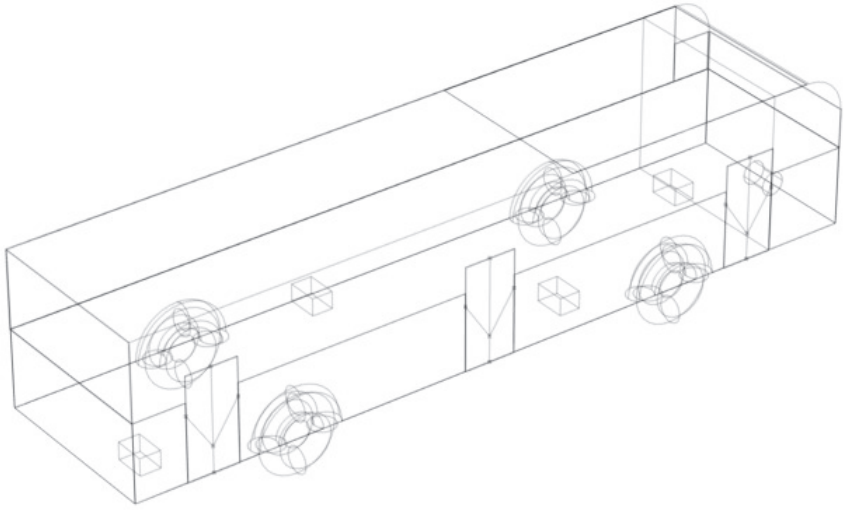

Figure 2: *Heater positions inside the electric bus*

A non-transparent view can be used for a better identification of some of the components, as in Figure 3, where the front door is selected to accentuate its position, dimensions, and properties. A 3D grid can be also displayed in order to estimate the spatial distribution of the components.

The last main component of the geometry model is the current collecting system of the electric bus. This system is placed on the vehicle roof and consists of two skates placed on two core bars, which assure the vehicle's energy supply when it operates in a non-autonomous way, like a trolley-bus (Figure 4).

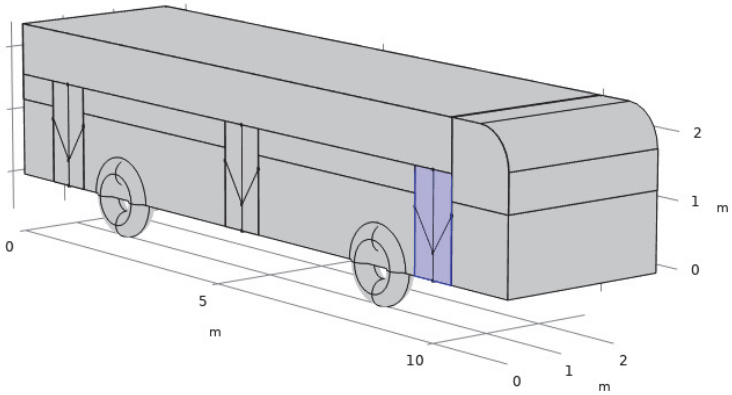

Figure 3: *Non-transparent view of the geometry model*

The finalized geometry has 87 domains, 676 boundaries, 1351 edges, and 773 vertices. This results in the basic geometry model of the electric bus, which will be used for the simulations.

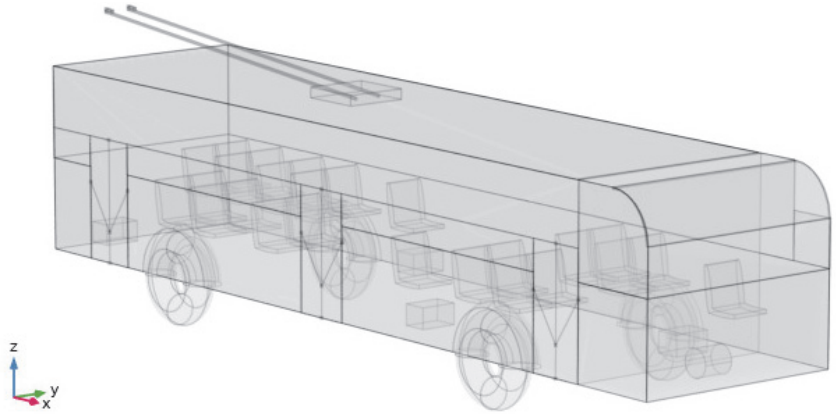

Figure 4: *The basic geometry model of the electric bus; transparent view*

The materials considered for the components of the bus for the model are iron, glass, acrylic plastic, fibreglass and PMMA – polymethyl methacrylate. The interior volume of the bus is modelled as filled with air.

4 SIMULATION RESULTS AND ANALYSIS

The main results of the simulations based on the thermal model are shown in Figure 5. Figure 5 shows the temperature distribution inside the electric bus with a view from the right side of the vehicle. The temperatures are estimated at the surfaces of the bus components. It can be observed that the highest temperature, as expected, is at the heaters (40 °C), and the lowest temperature is at the exterior surface of the roof, next to the power collecting box system where the trolleys are attached (17.3 °C).

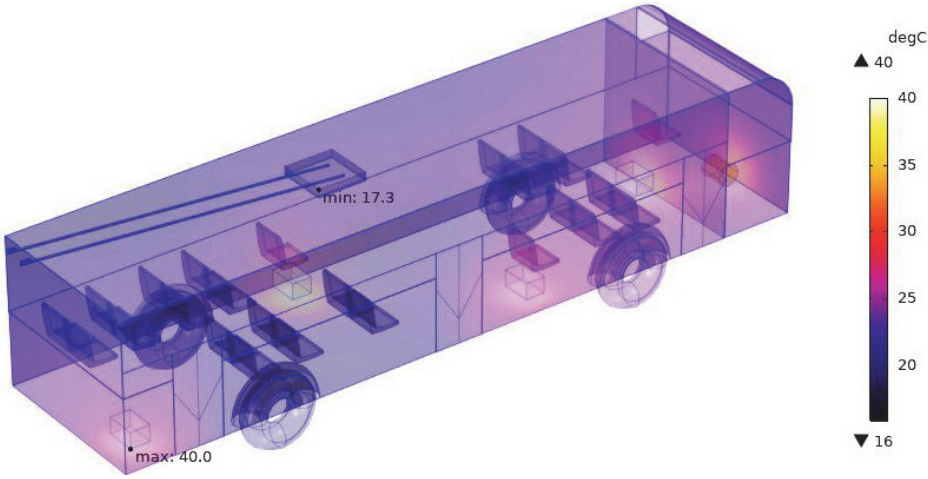

Figure 5: *Simulation results for the temperature distribution in the bus*

For a better visualization of the temperature distribution, it can be seen from the temperature variation along the electric bus that the higher temperatures are measured around the area where the heaters are placed and the lower temperature (between 17 °C and about 25 °C) in the area farthest from the heaters. For the validation of the thermal model, some experimental measurements of temperatures were taken at the various points in the interior of the electric bus. The results of the simulations were compared with the measured temperatures.

The temperatures were measured in different areas inside the electric bus with a point-and-shoot infrared camera (FLIR thermal-imaging camera). The temperature measured in the driver's cabin is 27.8 °C, quite comfortable for the driver. The temperature measured inside the electric bus, next to a heater, is 41.3 °C. These measurements are compared with the values resulting from the thermal simulation presented above. As seen in Figure 5, the simulated maximum temperatures inside the driver's cabin are between 25.2 °C and 27.9 °C, which are quite close to the measured temperature of 27.8 °C (Figure 6). As for the heaters, the simulated temperature is 40 °C, which is close to the measured one of 41.3 °C. Comparing the simulated and measured temperatures, it can be concluded that the thermal model of the electric bus can be validated as correct and be used further for a wide variety of simulation types in order to estimate the optimal solution to improve heat transfer inside the electric bus.

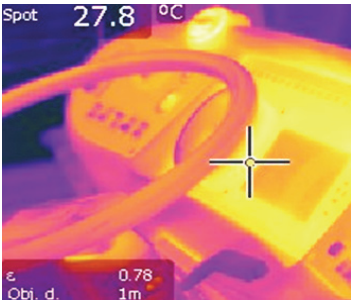

Figure 6: *Temperature measured with a thermal-imaging camera on the driver's cabin*

5 CONCLUSIONS

The geometry of an electric bus interior is designed considering the main components of the vehicle: passenger cabin, driver's cabin, windows, walls, seats and the main materials in accordance with a real bus. To study the heat transfer into the electric bus, a computer-aided design is used based on the heat transfer theory. A thermal model and simulations are made for the heat transfer inside the electric bus. The simulated data are compared with measurement data, and based on these data, it can be concluded that the thermal model of the electric bus can be validated and used further for various thermal simulations.

References

[1] **I. Evtimov, R. Ivanov, M. Sapundjiev:** *Energy consumption of auxiliary systems of electric cars*, MATEC web of conferences, EDP Sciences Vol. 133, p. 06002, 2017

[2] **M. Bartłomiejczyk, R. Kołacz:** *The reduction of auxiliaries power demand: The challenge for electromobility in public transportation*, Journal of Cleaner Production, 252, 119776, 2020

[3] **M. M., Hasan, J., Maasc, M. El Baghdadia, R. de Grootc, O. Hegazya:** *Thermal Management Strategy of Electric Buses towards ECO Comfort*, In proceedings of 8th Transport Research Arena Conference, TRA, 2020

[4] **H. Sahraei:** *Interior Climate U-Value calculation and optimization for electric buses at Volvo buses,* Master's thesis, Department of Mechanics and Maritime Sciences Chalmers University of Technology Gothenburg, Sweden, 2020

[5] **D. Göhlich, T.-A. Ly, A. Kunith, D. Jefferies:** *Economic assessment of different air-conditioning and heating systems for electric city buses based on comprehensive energetic simulations,* In EVS28 International Electric Vehicle Symposium and Exhibition, Kintex, Korea, May 3_6 (ed. Electric Vehicle Symposium (EVS)), 2015

[6] **M. Vražić, O. Barić, P. Virtič:** *Auxiliary systems consumption in electric vehicle*, *Przegląd* elektrotechniczny, Vol. 90, Iss. 12, p.p. 172-175, 2014

[7] **T. Zhang, C. Gao, Q. Gao, G. Wang, M. Liu, Y. Guo, Y.Y. Yan:** *Status and development of electric vehicle integrated thermal management from BTM to HVAC*, Applied Thermal Engineering, Vol. 88, p.p. 398-409, 2015

[8] **H. He, M. Yan, C. Sun, J. Peng, M. Li, H. Jia:** *Predictive air-conditioner control for electric buses with passenger amount variation forecast,* Applied energy, Vol. 227, p.p. 249-261, 2018

[9] **D. Göhlich, T. A. Fay, D. Jefferies, E. Lauth, A. Kunith, X. Zhang:** *Design of urban electric bus systems,* Design Science, Vol. 4, 2018

[10] **I. S. Suh, M. Lee, J. Kim, S.T. Oh, J.P. Won:** *Design and experimental analysis of an efficient HVAC (heating, ventilation, air-conditioning) system on an electric bus with dynamic on-road wireless charging*, Energy, Vol. 81, p.p. 262-273, 2015

[11] https://bkm.by/en/

[12] **V. Esanu, A. Motroi, I. Nuca, Iu. Nuca:** *Electrical Buses: Development and Implementation in Chisinau Municipality*, *Moldova*, 2019 International Conference on Electromechanical and Energy Systems (SIELMEN), 2019

Acknowledgement

This paper is a result of researches funded by the European Union on Joint Operational Programme Romania- Republic of Moldova – financed by the European Neighbourhood Instrument (ENI), Cross Border Cooperation (CBC), within the project: "ELBUS - Improving the cross-border public transportation using electric buses supplied with renewable energy", project reference number 2SOFT/3.1/54.

Nomenclature

(Symbols)	(Symbol meaning)
h	heat transfer coefficient, [W/m^{2}K]
k	thermal conductivity, [W/mK]
q	heat flux
T	temperature, [^{o}C]
T_s	temperature of the solid, [^{o}C]
T_f	temperature of the fluid, [^{o}C]
x	direction of the heat flux, [m]

JET Journal of Energy Technology

JET Volume 14 (2021) p.p. 57-71
Issue 2, October 2021
Type of article 1.04
www.fe.um.si/en/jet.html

DETERMINATION OF PRODUCED AND CONSUMED ELECTRICITY OF A RESIDENTIAL BUILDING USING A GRAPHICAL USER INTERFACE

DOLOČITEV PROIZVEDENE IN PORABLJENE ELEKTRIČNE ENERGIJE STANOVANJSKEGA OBJEKTA Z UPORABO GRAFIČNEGA UPORABNIŠKEGA VMESNIKA

Eva Simonič[1], Iztok Brinovar[1], Sebastijan Seme[1], Klemen Sredenšek[1✉]

Keywords: graphical user interface, photovoltaic system, heat pump, production of electricity, consumption of electricity

Abstract

The primary objective of this paper is to present a graphical user interface for the calculation of electricity produced by a photovoltaic system and electricity consumed by a heat pump. The produced electricity is determined by a multi-year average of measurements of the global and diffuse power density of solar radiation for several places in Slovenia, while consumed electricity is determined based on the required heat for heating a residential building and domestic water. The calculation of produced and consumed electricity is validated by measurements on a real system. The developed graphical user interface enables simple user inputs of the photovoltaic system, heat pump, and the considered residential building, and provides a comprehensive technical analysis for installing both systems at the same location.

✉ Corresponding author: Klemen Sredenšek, M.Sc., E-mail address: klemen.sredensek@um.si

[1] University of Maribor, Faculty of Energy Technology, Hočevarjev trg 1, 8270 Krško, Slovenia

Povzetek

Glavni cilj tega prispevka je predstavitev grafičnega uporabniškega vmesnika za izračun proizvedene električne energije s fotonapetostnim sistemom in porabljene električne energije s toplotno črpalko. Predvidena proizvedena električna energija je določena z večletnimi povprečji meritev globalne in difuzne gostote moči sončnega sevanja za več krajev po Sloveniji, medtem ko je poraba električne energije določena na podlagi toplote za ogrevanje stavbe in sanitarne tople vode. Izračun proizvedene in porabljene električne energije je ovrednoten z meritvami na realnem sistemu. Izdelan grafični uporabniški vmesnik predvideva preproste uporabniške vnose fotonapetostnega sistema, toplotne črpalke in obravnavanega objekta ter podaja celovito tehnično analizo za postavitev obeh sistemov hkrati.

1 INTRODUCTION

An increasing number of households are opting for alternative heating solutions for residential buildings in a bid to achieve a higher level of self-sufficiency. One example of a modern solution is the use of a heat pump for heating a building and sanitary water, which increases the share of renewable energy sources (RES). Additionally, the necessary electricity for operation of the heat pump can be produced by a photovoltaic (PV) system installed on the residential building itself. This increases the level of self-sufficiency of the household. The decision to invest in a combination of a PV system and a heat pump for heating purposes is simpler if it is supported by appropriate forecast calculations. To this end, investors can use a graphical user interface that calculates produced and consumed electricity for any residential building based on simple user inputs. Based on the idea of the described graphical user interface, this paper is divided into two parts: a calculation of electricity production using a PV system, and electricity consumption with a heat pump. The authors [1] found that the electricity produced by the PV system is directly dependent on the solar radiation received and the apparent position of the Sun in the sky. One option is to rely on local measurements from previous years to predict solar radiation at any point on Earth [2]. In Slovenia, these measurements are provided by ARSO (Environmental Agency of the Republic of Slovenia) [3]. Many authors, such as [1–2, 4–7], present different models for determining solar radiation of any surface on Earth based on knowledge of the power density of solar radiation on a horizontal surface and geometric relationships between the Earth and the Sun. The requirements of the methodology for calculating the energy performance of buildings and providing their own RES for the operation of systems in buildings [8] are set out by the Rules on the Efficient Use of Energy in Buildings (PURES) [8]. The requirements are followed and explained by the Technical Guidelines for Construction TSG-1-004: 2010 Energy efficiency [9].

The latter also provides a methodology for calculating the electricity required to operate a heat pump. By conducting this research, the authors are pursuing a goal of creating a graphical user interface in the Matlab software package. The established methods for calculating the production and consumption of electricity and the search for simplification were taken into account, which would also meet user input restrictions and ensure the greatest possible automation of the calculation. Existing graphical user interfaces in the field of PV systems, such as [10], are primarily intended for PV system sizing or daily solar radiation forecasts, as described by the authors [11]. In the field of inspection of buildings, in terms of heating, the KI Energija programme [12] stands out, which also follows the PURES. In addition to the above, the RETScreen clean energy management software package [13] is available on the market, which

deals with technical and financial energy efficiency analysis. After reviewing the literature, it was found that the proposed graphical user interface represents an innovative approach to evaluating the considered systems and user information.

This paper consists of four sections. The first section provides an introduction to the research topic. The second section describes the methodology of production and consumption of electricity, while the third section presents the results of the graphical user interface and the validation with measurements. The fourth and final section discusses the conclusions of the paper.

2 METHODOLOGY

The first subsection covers the basics of solar radiation, the calculation of solar radiation on the surface, and the necessary geometric connections between the Sun and the Earth. The second subsection deals with the calculation of the electricity required for the operation of the heat pump.

2.1 Production of electricity – PV system

The power density of solar radiation at the edge of the Earth's atmosphere and the Earth's average distance from the Sun is called the solar constant, which is approximately 1366 W/m^2 [14, 15]. Horizontal surfaces on Earth receive two types of solar radiation: direct solar radiation $I_{b,h}$, which does not experience a significant change in direction on the way through the atmosphere [2], and diffuse solar radiation $I_{d,h}$, which results from the scattering of sunlight in the atmosphere [16]. The greater the scatter, the smaller the direct component of solar radiation and vice versa [16]. The sum of direct and diffuse solar radiation is the global solar radiation on the horizontal surface I_h and is given by (2.1) [2].

$$I_h = I_{b,h} + I_{d,h} \tag{2.1}$$

In addition to global solar radiation, an arbitrarily directed surface also receives reflected radiation $I_{r,c}$, which results from the reflection of global solar radiation from the environment [2]. The total radiation on any surface is thus the sum of direct, diffuse and reflected solar radiation on any surface expressed by (2.2) [2].

$$I_c = I_{b,c} + I_{d,c} + I_{r,c} \tag{2.2}$$

To calculate the solar radiation of an arbitrarily oriented surface at any location on Earth, it is necessary to understand the geometric relationship between the Earth and the Sun in a selected period of time. The distance of the Earth from the Sun changes throughout the year. The Earth is closest to the Sun at the winter solstice (21 December) and furthest from the Sun at the summer solstice (21 June). At that time, the declination takes its extreme values, representing the angle between the conjunction of the centres of the Earth and the Sun and the plane of the Earth's equator. The declination for an individual day of the year is calculated according to (2.3) [6].

$$\delta = 23{,}45 \cdot \sin\left[\frac{360 \cdot (284 + n)}{365}\right] \tag{2.3}$$

The apparent current height of the Sun in the sky is described by the solar altitude angle α [1]. The solar altitude angle is the angle between direct sunlight and the horizontal surface of the Earth, calculated by (2.4) [4].

$$\alpha = \sin^{-1}\left(\sin L \sin\delta + \cos L \cos\delta \cos h\right) \tag{2.4}$$

The angle between the direct sunlight and the normal of the considered surface is called the incidence angle of the Sun i [5] and is calculated by (2.5) [7].

$$i = \cos^{-1}\left(\begin{array}{c}\sin L \sin\delta \cos\beta - \cos L \sin\delta \cos\gamma \\ + \cos L \cos\delta \cos h \cos\beta + \sin L \cos\delta \cos h \sin\beta \cos\gamma \\ + \cos\delta \sin h \sin\beta \sin\gamma\end{array}\right) \tag{2.5}$$

As previously mentioned, the total solar radiation I_c as well as the solar irradiation H_c (expressed by (2.6)) received by any surface is the sum of direct, diffuse and reflected solar irradiation, taking into account the corresponding inclination factor for each radiation component (2.7), (2.8) and (2.9) [2].

$$H_c = R_b B_h + R_d D_h + R_r\left(B_h + D_h\right) \tag{2.6}$$

$$R_b = \frac{\cos i}{\sin\alpha} \tag{2.7}$$

$$R_d = \frac{1 + \cos\beta}{2} \tag{2.8}$$

$$R_r = \frac{\rho\left(1 - \cos\beta\right)}{2} \tag{2.9}$$

2.2 Consumption of electricity – heat pump

The main goal of a building heating system is to provide internal thermal comfort [8]. The most popular heating devices or heat generators currently on the market are so-called heat pumps, which use the temperature of the environment to produce heat for heating and are electricity operated. The electricity required for operation of a heat pump is calculated by (2.10) [9].

$$E_{HP} = \frac{Q_{HP}}{COP} \tag{2.10}$$

The indoor design temperature T_i = 20 °C was used to calculate the daily heat required for heating. The author in [9] assumes that this value is the same as the indoor design temperature for determining the annual heat required for heating residential buildings. The required daily heat $Q_{NH,n}$ is calculated by (2.11).

$$Q_{NH,n} = \left(Q_{trans,n} + Q_{v,n}\right) - \eta_{NH}\left(Q_{i,n} + Q_{s,n}\right) \tag{2.11}$$

Transmission heat losses occur due to the heat transfer through building structures [9]. Heat transfer through building structures occurs due to the temperature difference between indoor

and outdoor air, with heat passing through three heat transfer mechanisms (convective heat transfer, conductive heat transfer, and radiation). Indoor heat is transferred to the inner surface of a building envelope by radiation and convection. Heat is transferred to the outer surface through the layers of building structures, and is then re-transferred by radiation and convection to the surrounding air. Heat transfer by radiation and convection is combined and presented by internal α_i and external α_e convective heat transfer coefficient. The thermal transmittance of a building structure is expressed by (2.12) by considering all three heat transfer mechanisms [37, 38].

$$U = \frac{1}{\frac{1}{\alpha_i} + \sum_{j=1}^{n} \frac{d_j}{\lambda_j} + \frac{1}{\alpha_e}} \tag{2.12}$$

According to [17], the external convective heat transfer coefficient α_e is 25 W/m^{2}K for all heat flow directions. However, the internal heat transfer coefficient α_i is 7.69 W/m^{2}K in the horizontal direction of heat flow, 10 W/m^{2}K in the upwards direction of heat flow, and 5.88 W/m^{2}K in the downwards direction of heat flow. The coefficient of specific transmission heat losses of an entire building envelope is determined by (2.13).

$$H_t^{'} = \frac{\sum_{j=1}^{n} U_j A_j}{\sum_{j=1}^{n} A_j} + 0{,}06 \tag{2.13}$$

The last term in (2.13) represents an increase in the thermal transmittance of the building envelope by 0.06 due to the influence of thermal bridges [9]. Transmission heat losses for a given day of the year are then calculated by (2.14).

$$Q_{trans,n} = H_t \left(T_i - T_{e,n}\right) t \tag{2.14}$$

The coefficient of specific transmission heat losses H_t is calculated by (2.15) [8, 9].

$$H_t = H_t^{'} \cdot A \tag{2.15}$$

Ventilation heat losses for a given day of the year are calculated by (2.16).

$$Q_{v,n} = H_v \left(T_i - T_{e,n}\right) t \tag{2.16}$$

The coefficient of ventilation heat losses is calculated by (2.17).

$$H_v = 0{,}34 \cdot k \cdot V_{neto} \tag{2.17}$$

The heat gains of internal sources Q_i are due to the movement of people, the operation of devices, and lighting in the room. For residential buildings, the usable area of the building A_u is simplified to 4 W/m^2 [9]. Heat gains due to solar radiation on a given day $Q_{s,n}$ are calculated by (2.18).

$$Q_{s,n} = H_{c,n} \cdot F_s \cdot F_c \cdot F_f \cdot A_{window} \cdot g \tag{2.18}$$

It was assumed that there is no shading of windows with external obstacles (shading factor F_s = 1) and that blinds are not in use during the heating period (blinds factor F_c = 1). The window

frame factor specifies the proportion of glazing on the entire window surface. In the event that the window frame factor is unknown, the value F_f = 0.7 is assumed after [9]. The efficiency of heat gains η_{NH} by the monthly method is given by (2.19).

$$\eta_{NH,m} = \frac{1-\gamma_{H,m}^{a_H}}{1-\gamma_{H,m}^{a_H+1}} \tag{2.19}$$

The ratio between heat gains and heat losses $\gamma_{H,m}$ is given by (2.20), where the parameter m represents the month of the year.

$$\gamma_{H,m} = \frac{Q_{i,m}+Q_{s,m}}{Q_{trans,m}+Q_{v,m}} \tag{2.20}$$

The dimensionless parameter a_H is given by (21).

$$a_H = 1+\frac{\tau}{15} \tag{2.21}$$

The time constant of the building τ, presented in (2.21) is given by (2.22) according to a simplified method.

$$\tau = \frac{50\cdot V}{H_t+H_v} \tag{2.22}$$

If the heat pump is also used for domestic water heating, the heat output of the heat pump is calculated by (2.23) according to the simplified calculation.

$$Q_{HP} = Q_{NH}+Q_w \tag{2.23}$$

The heat required to calculate the domestic hot water Q_w presented in (2.23) is calculated by (2.24) [9], where the specific annual energy consumption for domestic hot water q_w presented in (2.24) is 12 kWh/m^2/year for single-family houses [9].

$$Q_w = \frac{q_w}{365} d_w A_u \tag{2.24}$$

3 RESULTS AND DISCUSSION

3.1 Validation of electrical (PV system) and thermal model (heat pump) with measurements

Validation of the electrical model or methodology for calculating the electricity production of the PV system was performed based on measurements on a real PV system in the vicinity of Krško, Slovenia. The PV system consists of six single-crystal PV modules (72 PV cells) with an average selected efficiency of 15 %. The PV system is oriented to the south (a_w = 0 °) at an inclination angle of β = 30° with a total area of 6.75 m^2. To confirm the electrical model of the graphical user interface, a comparison was made between the results of the electrical model and the measurements on the presented PV system (Figure 1).

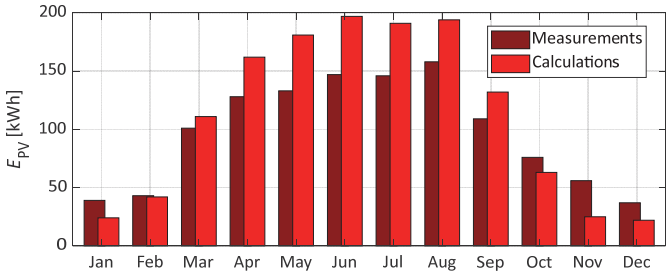

Figure 1: *Validation of electrical model (production of electricity from PV system) with measurements.*

Figure 1 shows that there are minor deviations in February, March and October. Significant deviations can be observed in the summer months from 17-26 %. The annual deviation between the calculated and measured electricity production is 12.72 %. The deviations are a consequence of measurement data of global and diffuse solar radiation, constant efficiency of the PV system, disregard for shading of surrounding buildings and that of degradation of the PV system, which occurs with the increase of the lifetime of the PV system. Validation of the thermal model or methodology for calculating the electricity consumption of the heat pump for heating the building was performed on the basis of measurements on a real residential building in the vicinity of Maribor, Slovenia. The residential building has a heating volume of 553.6 m^3, using an air-to-water heat pump. To confirm the thermal model of the graphical user interface, a comparison was made between the thermal model results and the measurements on the presented residential building (Figure 2).

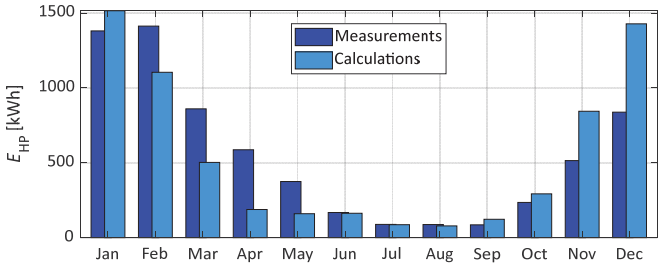

Figure 2: *Validation of thermal model (consumption of electricity by heat pump) with measurements.*

Figure 2 shows minor deviations in the summer months, when only domestic hot water is heated. A significant deviation can be seen when comparing individual months, while the annual deviation between the calculated and measured electricity consumption is only 2.25 %. The deviations are due to the simplification of the calculation of electricity consumption (neglect of heat losses of the heating system and hot water system) and the assumption of constant values of internal design temperature and a number of air exchanges (depending mainly on the living habits of residents).

3.2 Presentation of graphical user interface

The created graphical user interface is divided into four tabs. The first tab presents the data entry for calculating solar radiation and electricity production of the PV system (Figure 3). The user has the option of choosing between eleven locations across Slovenia, which are evenly spaced. Based on the choice of location, relevant meteorological data are determined, namely, a multi-year average of half-hour power density measurements of global and diffuse solar radiation [3], and average daily temperature summarised after a typical meteorological year. The average daily temperature is also used in the calculation of building heat losses. The choice of location also prescribes the corresponding latitude *L*, used to calculate the solar altitude angle α (2.5) and the angle of incidence of the Sun's rays *i* (2.6).

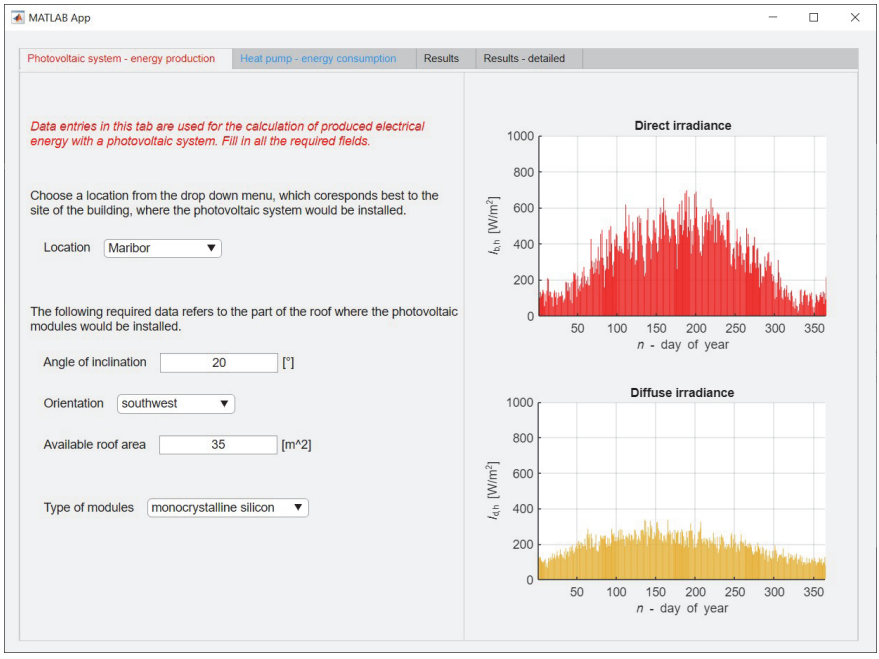

Figure 3: *First tab 'Photovoltaic system – production of electricity'*

The second tab represents the data entry for calculating the heat consumption of the heat pump. The second tab is divided into six sub-tabs for more detailed analysis. In the first sub-tab, shown in Figure 4, a simple or difficult data entry can be selected.

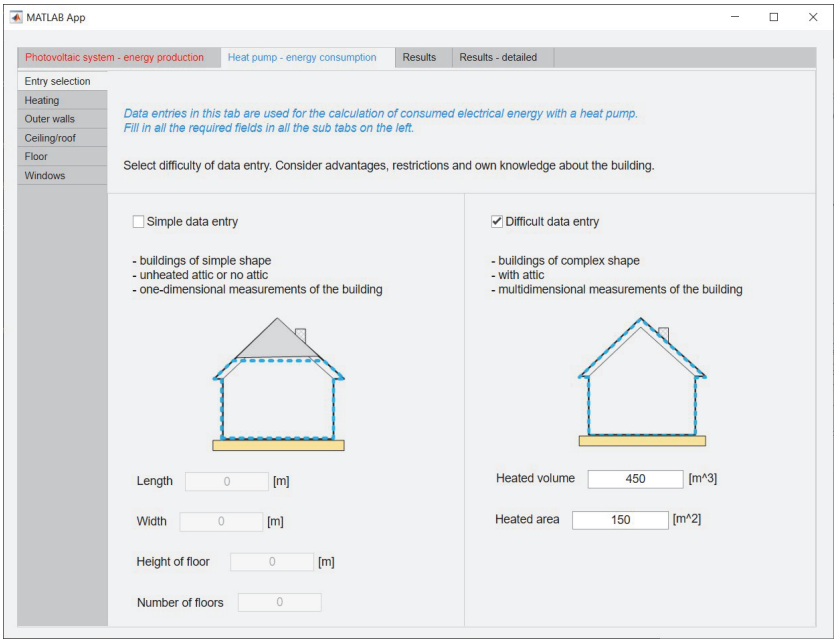

Figure 4: *Second tab 'Heat pump – consumption of electricity'*

Simple data entry is intended for buildings of simple geometric shape without an attic or with an unheated attic. Thus, the outer envelope of a building approaches the shape of a square, and the one-dimensional dimensions of a building can determine a building's gross heated volume and usable area. The required user entries are the length and width of the building, the height of the floor, and the number of floors. The difficult data entry is intended for buildings of complex shapes, which may also have an attic. In this case, the user must know the multidimensional dimensions of the building and determine the gross heated volume, usable area and areas of individual elements of the external envelope of the building. The calculation with difficult data entry is more accurate but requires better knowledge of the building. The 'Heating' sub-tab allows the selection of heat pump type, the outlet water temperature, and whether the heat pump includes domestic hot water heating. The 'Heat pump type' drop-down list offers air-to-water, water-to-water, and brine-to-water options. In the 'Outlet water temperature' drop-down list, the user selects between 35 °C and 55 °C, which corresponds to the type of heaters in the building. The type of heat pump and the outlet water temperature are necessary data for determining the heating number of the coefficient of performance (COP). The sub-tabs 'Outer walls', 'Ceiling/roof' and 'Floor' (shown in Figure 5) are intended to determine the composition of individual elements of a building's exterior envelope. The composition of the outer envelope is determined by the choice of materials and their thicknesses. Materials are divided into seven categories: walls, mortars, stone and earth, fillers, concretes, thermal insulators, and cladding.

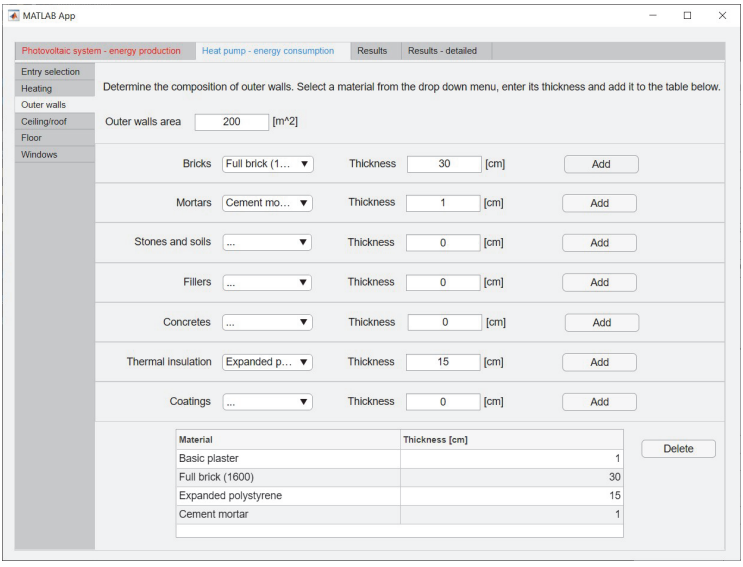

Figure 5: *Sub-tab 'Outer walls'*

The 'Windows' sub-tab (shown in Figure 6) allows entry of thermal transmittance of windows, the solar energy transmittance of glass *g*, a window area, and their orientation.

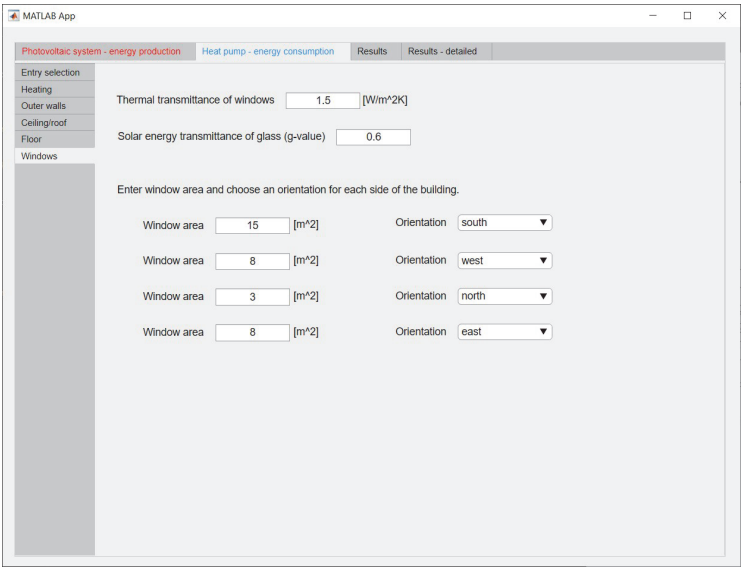

Figure 6: *Sub-tab 'Windows'*

The 'Results' tab (Figure 7) shows the calculated produced and consumed electricity on a monthly and annual basis, while the 'Results – detailed' tab (Figure 8) shows some additional calculated quantities.

Figure 7: *Third tab 'Results – produced and consumed electricity'*

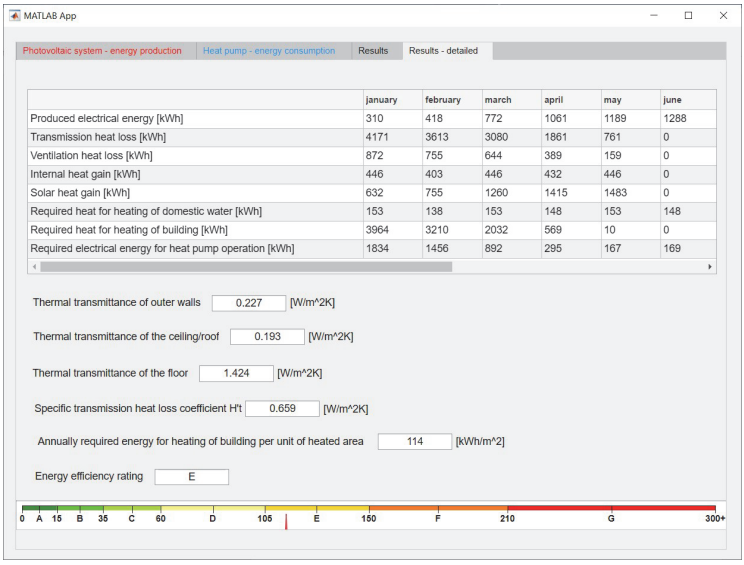

Figure 8: *Fourth tab 'Results detailed – energy efficiency rating'*

The tab 'Results – detailed' (Figure 8) shows the monthly and annual values of the following calculated values: produced electricity, transmission heat losses, ventilation heat losses, internal heat gain, solar heat gain, required heat for heating of domestic water, required heat for heating of the building, and required electricity for heat pump operation. Below the table, the calculated thermal transmittances of each element of the building envelope and the

coefficient of specific transmission losses are displayed. Additionally, the annual required energy for heating of building per unit of heated area is calculated and shown, based on which the energy efficiency rating is determined. The criterion for determining the energy efficiency rating is determined based on [37]. In addition, the corresponding letter of the energy efficiency rating of the building is displayed, with the pointer showing the appropriate place on the colour scale of the energy classes.

4 CONCLUSION

This paper presents a graphical user interface for calculating electricity produced by a photovoltaic system and electricity consumed by a heat pump. The aim of the paper is to create an accurate tool to analyse the current and future technical view of residential buildings with a user-friendly and straightforward designed graphical user interface. Required meteorological data was obtained by the Environmental Agency of Slovenia, while other data were summarised according to technical guidelines for energy efficiency in buildings. The discussed methodology for the calculation of produced and consumed electricity was validated with measurements on a real system. In addition, it is essential to highlight the minimum deviations between the methodology results and measurements, which ranged from 2.25 % (for consumed electricity) to 12.72 % (for produced electricity).

References

[1] **K. Jazayeri, S. Uysal, M. Jazayeri:** *MATLAB/simulink based simulation of solar incidence angle and the sun's position in the sky with respect to observation points on the Earth*, International Conference on Renewable Energy Research and Applications (ICRERA), p.p. 173-177, 2013

[2] **D. Y. Goswami, F. Kreith, J. F. Kreider:** *Principles of solar engineering*, 2nd edition, New York: Taylor & Francis Group, 2000

[3] Available: https://www.meteo.si/met/sl/archive/. [11.10.2021]

[4] **S. Wang:** *In-Plane Solar Irradiance Calculation for Various Type of PV Arrays*, IEEE 46th Photovoltaic Specialists Conference (PVSC), p.p. 1,645-1,648, 2019

[5] **S. K. Jha, S. Roy, V. K. Singh, D. P. Mishra:** *Sun's Position Tracking by Solar Angles Using MATLAB*, International Conference on Renewable Energy Integration into Smart Grids: A Multidisciplinary Approach to Technology Modelling and Simulation (ICREISG), p.p. 5-9, 2020

[6] **Y. Dong, L. Xu, M. Lu, M. Ding, B. Wu:** *Design optimization of photovoltaic (PV) array optimum tilt*, China International Conference on Electricity Distribution (CICED), p.p. 1,028-1,032, 2014

[7] **D. Lenardič:** Photovoltaic systems: handbook: building blocks, planning, installation and maintenance, 2nd edition, Ljubljana: Agencija Poti, 2012

[8] Rules on the Efficient Use of Energy in Buildings. Official Gazette of the Republic of Slovenia, no.52, p. 7,840, 2010

[9] **Ministry of the Environment and Spatial Planning of the Republic of Slovenia**. Technical Guidelines for Construction TSG-1-004: 2010 Energy efficiency (22 June 2010). Available: http://www.arhiv.mop.gov.si/fileadmin/mop.gov.si/pageuploads/zakonodaja/prostor/graditev/TSG-01-004_2010.pdf. [11.10.2021]

[10] **A. S. Mohd Nordin, A. F. M. Nor:** *Development of a Graphical User Interface (GUI) Platform for Sizing a Grid-Connected Photovoltaic (PV) System*, Evolution in Electrical and Electronic Engineering, vol.1, no.1, p.p. 15-24, 2020

[11] **S. Ç. Bektaş, R. Çakmak, İ. H. Altaş:** *Design of a MATLAB GUI for Day Ahead Forecasting of PV Panel Power*, Innovations in Intelligent Systems and Applications Conference (ASYU), p.p. 1-5, 2019

[12] Available: https://www.knaufinsulation.si/program-ki-energija-2017. [11.10.2021]

[13] Available:https://www.nrcan.gc.ca/maps-tools-and-publications/tools/modelling-tools/retscreen/7465. [11.10.2021]

[14] **H. Zirin, K. Lang:** *Sun: Physical properties* (4 February 2021). Encyclopedia Britannica. Available: https://www.britannica.com/place/Sun. [11.10.2021]

[15] **H. Zirin, K. Lang:** *Solar constant.* (24.8.2012). Encyclopedia Britannica. Available: https://www.britannica.com/science/solar-constant. [11.10.2021]

[16] **D. Kastelec, J. Rakovec, K. Zakšek:** *Solar energy in Slovenia,* Ljubljana: ZRC Publishing House, ZRC SAZU, 2007

[17] **M. Z. Degefa, M. Lehtonen, K. Nixon, M. McCulloch:** *A high resolution model of residential internal heat gain – The subtle interdependencies among residential end uses*, IEEE Innovative Smart Grid Technologies - Asia (ISGT ASIA), p.p. 1-6, 2015

Nomenclature

(Symbols)	(Symbol meaning)
A	the area of the outer envelope of a building
a_H	dimensionless parameter
A_u	usable area of building
A_{window}	window area
B_h	direct solar irradiation on horizontal surface
d	layer thickness of the building structure
D_h	diffuse solar irradiation on horizontal surface
d_w	the number of days of hot water supply in a given period
E_{HP}	required electricity for the operation of the heat pump
F_c	blinds factor
F_f	frame factor

F_s	shading factor
g	solar radiation transmittance factor
h	hour angle
H_c	total solar irradiation on observed surface
$H_{c,n}$	total solar irradiation of observed surface for the selected day of the year
H_t	coefficient of transmission heat losses
H_t'	coefficient of specific transmission heat losses
H_v	coefficient of ventilation heat losses
i	incidence angle of the sun
$I_{b,c}$	power density of direct solar radiation on an inclined surface
$I_{b,h}$	power density of direct solar radiation on a horizontal surface
I_c	power density of total solar radiation on an inclined surface
$I_{d,c}$	power density of diffuse solar radiation on an inclined surface
$I_{d,h}$	power density of diffuse solar radiation on a horizontal surface
I_h	power density of global solar radiation on a horizontal surface
$I_{r,c}$	power density of reflected solar radiation on an inclined surface
k	number of air exchanges
L	latitude
m	consecutive month of the year
n	consecutive day of the year
η_{NH}	efficiency of heat gains
$\eta_{NH,m}$	efficiency of heat gains for the selected month of the year
Q_{HP}	heat produced for heating
Q_i	heat gains from internal sources
$Q_{i,m}$	heat gains from internal sources for the selected month of the year
$Q_{i,n}$	heat gains from internal sources for the selected day of the year
Q_{NH}	heat required to heat the building
$Q_{NH,n}$	heat required to heat the building for the selected day of the year
$Q_{s,m}$	heat gains due to solar radiation for the selected month of the year
$Q_{s,n}$	heat gains due to solar radiation for the selected day of the year
$Q_{trans,m}$	transmission heat losses for the selected month of the year
$Q_{trans,n}$	transmission heat losses for the selected day of the year

$Q_{v,m}$	ventilation heat losses for the selected month of the year
$Q_{v,n}$	ventilation heat losses for the selected day of the year
Q_w	heat required to heat hot water
q_w	specific annual energy use for hot water
R_b	inclination factor for direct solar irradiation
R_d	inclination factor for diffuse solar irradiation
R_r	inclination factor for reflected solar irradiation
t	time period
$T_{e,n}$	average daily outdoor temperature for the selected day of the year
T_i	indoor design temperature
U	thermal transmittance
V	gross heated volume of the building
V_{neto}	net heated volume of the building
α	solar altitude angle
α_e	external convective heat transfer coefficient
α_i	internal convective heat transfer coefficient
β	inclination angle
γ	azimuth angle
$\gamma_{H,m}$	the ratio between heat gains and heat losses for the selected month of the year
δ	declination angle
λ	thermal conductivity
ρ	reflection factor
τ	the time constant of the building

JET Journal of Energy Technology

Author instructions

www.fe.um.si/en/jet.html

MAIN TITLE OF THE PAPER
SLOVENIAN TITLE

*Author[1], Author [2], Corresponding author*ℜ

Keywords: (Up to 10 keywords)

Abstract

Abstract should be up to 500 words long, with no pictures, photos, equations, tables, only text.

Povzetek

(Abstract in Slovenian language)

Submission of Manuscripts: All manuscripts must be submitted in English by e-mail to the editorial office at jet@um.si to ensure fast processing. Instructions for authors are also available online at http://www.fe.um.si/en/jet/author-instructions.html.

Preparation of manuscripts: Manuscripts must be typed in English in prescribed journal form (MS Word editor). A MS Word template is available at the Journal Home page.

A title page consists of the main title in the English and Slovenian language; the author(s) name(s) as well as the address, affiliation, E-mail address, telephone and fax numbers of author(s). Corresponding author must be indicated.

Main title: should be centred and written with capital letters (ARIAL bold 18 pt), in first paragraph in English language, in second paragraph in Slovenian language.

Key words: A list of 3 up to 6 key words is essential for indexing purposes. (CALIBRI 10pt)

Abstract: Abstract should be up to 500 words long, with no pictures, photos, equations, tables, - text only.

Povzetek: - Abstract in Slovenian language.

Main text should be structured logically in chapters, sections and sub-sections. Type of letters is Calibri, 10pt, full justified.

ℜ Corresponding author: Title, Name and Surname, Organisation, Department, Address, Tel.: +XXX x xxx xxx, E-mail address: x.x@xxx.xx

[1] Organisation, Department, Address

[2] Organisation, Department, Address

Units and abbreviations: Required are SI units. Abbreviations must be given in text when first mentioned.

Proofreading: The proof will be send by e-mail to the corresponding author in MS Word's Track changes function. Corresponding author is required to make their proof corrections with accepting or rejecting the tracked changes in document and answer all open comments of proof reader. The corresponding author is responsible to introduce corrections of data in the paper. The Editors are not responsible for damage or loss of submitted text. Contributors are advised to keep copies of their texts, illustrations and all other materials.

The statements, opinions and data contained in this publication are solely those of the individual authors and not of the publisher and the Editors. Neither the publisher nor the Editors can accept any legal responsibility for errors that could appear during the process.

Copyright: Submissions of a publication article implies transfer of the copyright from the author(s) to the publisher upon acceptance of the paper. Accepted papers become the permanent property of "Journal of Energy Technology". All articles published in this journal are protected by copyright, which covers the exclusive rights to reproduce and distribute the article as well as all translation rights. No material can be published without written permission of the publisher.

Chapter examples:

1 MAIN CHAPTER

(Arial bold, 12pt, after paragraph 6pt space)

1.1 Section

(Arial bold, 11pt, after paragraph 6pt space)

1.1.1 Sub-section

(Arial bold, 10pt, after paragraph 6pt space)

Example of Equation (lined 2 cm from left margin, equation number in normal brackets (section. equation number), lined right margin, paragraph space 6pt before in after line):

Equation (1.1)

Tables should have a legend that includes the title of the table at the top of the table. Each table should be cited in the text.

Table legend example:

Table 1: *Name of the table (centred, on top of the table)*

Figures and images should be labelled sequentially numbered (Arabic numbers) and cited in the text – Fig.1 or Figure 1. The legend should be below the image, picture, photo or drawing.

Figure legend example:

Figure 1: *Name of the figure (centred, on bottom of figure, photo, or drawing)*

References

[1] **N. Surname:** *Title,* Journal Title, Vol., Iss., p.p., Year of Publication

[2] **N. Surname:** *Title,* Publisher, Year of Publication

[3] **N. Surname:** *Title* [online], Publisher or Journal Title, Vol., Iss., p.p., Year of Publication. Available: website (date accessed)

Examples:

[1] **J. Usenik**: *Mathematical model of the power supply system control*, Journal of Energy Technology, Vol. 2, Iss. 3, p.p. 29 – 46, 2009

[2] **J. J. DiStefano, A.R. Stubberud, I. J. Williams**: *Theory and Problems of Feedback and Control Systems*, McGraw-Hill Book Company, 1987

[3] **T. Žagar, L. Kegel:** *Preparation of National programme for SF and RW management taking into account the possible future evolution of ERDO* [online], Journal of Energy Technology, Vol. 9, Iss. 1, p.p. 39 – 50, 2016. Available: http://www.fe.um.si/images/jet /Volume 9_Issue1/03-JET_marec_2016-PREPARATION_OF_NATIONAL.pdf (7. 10. 2016)

Example of reference-1 citation: In text *[1],* text continue.

Nomenclature

(Symbols)	(Symbol meaning)
t	time

JET

JET I Journal of Energy Technology I Vol. 14, Issue 2, October 2021 I University of Maribor, Faculty of Energy Technology

ISSN 1855-5748

9 771855 574008